

# How Trustworthy are the Existing Performance Evaluations for Basic Vision Tasks?

Hamid RezaTofighi<sup>1,2\*</sup> Tran Thien Dat Nguyen<sup>3\*</sup> Ba-Ngu Vo<sup>3</sup> Ba-Tuong Vo<sup>3</sup>  
Silvio Savarese<sup>4</sup> Ian Reid<sup>2</sup>

<sup>1</sup>Monash University <sup>2</sup>University of Adelaide <sup>3</sup>Curtin University <sup>4</sup>Stanford University  
hamid.rezatofighi@monash.edu; t.nguyen172@postgrad.curtin.edu.au

## Abstract

*Performance evaluation is indispensable to the advancement of machine vision, yet its consistency and rigour have not received proportionate attention. This paper examines performance evaluation criteria for basic vision tasks namely, object detection, instance-level segmentation and multi-object tracking. Specifically, we advocate the use of criteria that are (i) consistent with mathematical requirements such as the metric properties, (ii) contextually meaningful in sanity tests, and (iii) robust to hyper-parameters for reliability. We show that many widely used performance criteria do not fulfill these requirements. Moreover, we explore alternative criteria for detection, segmentation, and tracking, using metrics for sets of shapes, and assess them against these requirements.*

## 1. Introduction

In addition to technological and algorithmic developments, performance evaluation is indispensable to the advancement of machine vision. It is difficult to envisage how improvements and/or advances can be made and demonstrated without performance evaluation. In this work we restrict ourselves to basic vision tasks such as object detection, instance-level segmentation, and multi-object tracking, where several benchmarks have been proposed to evaluate their performance [5, 7, 12, 15, 19, 20, 34, 39, 41, 44, 53]. The ensuing scientific questions are: how trustworthy are these performance evaluation methods, and how to formulate ‘trustworthy’ performance evaluation strategies?

Given the importance of performance evaluation, its consistency and rigour have not received proportionate attention in computer vision. The standard practice is to rank the solutions according to certain criteria based on their outputs or *predictions/estimates* on prescribed

datasets [19, 34, 39]. In general, these criteria aim to capture the similarities/dissimilarities between the *predictions* and prescribed *references*, with higher similarities indicating better performance. In practice, performance criteria are chosen, largely, via intuition (*e.g.* see [5, 32, 39]), rather than through a formal process.

This paper attempts to provide some formalism for performance evaluation of basic computer vision tasks. Intuition is important in the formulation of performance criteria, but does not necessarily guarantee fairness and consistency. Hence, mathematical considerations and systematic testing on purposefully constructed scenarios are needed to ascertain fairness and consistency while capturing the intent behind the intuition. Our contributions toward such formalism are as follows.

1. We advocate the following guidelines for validating *trustworthiness* of performance criteria:

- (i) suitable analytical properties, *e.g.* metric properties to warrant mathematical consistency;
- (ii) meaningful in *sanity tests*—systematically constructed test scenarios with pre-determined rankings—to capture the intent of the evaluation;
- (iii) robust to variations in hyper-parameters for reliability.

2. For popular basic vision performance criteria, such as F1, log-Average Miss Rate, mean Average Precision, Multi-Object Tracking Accuracy, and IDF1, we demonstrate: (i) they are not mathematically consistent, *i.e.* not metric; (ii) their rankings of predictions are not consistent in sanity tests; and (iii) their rankings can change dramatically with different choices of hyper-parameters.

3. We suggest (*mathematical*) *metrics* for sets of shapes as alternative performance criteria for object detection, instance-level segmentation, and multi-object tracking, by integrating point pattern metrics with shape metrics. We also assess these metrics (together with the above performance criteria) against the suggested guidelines to determine the most trustworthy criterion.

\*indicates equal contribution

## 2. Related work

Several performance evaluation methods have been proposed for the basic vision tasks: object detection; instance level segmentation; and multi-object tracking.

**Intersection over Union (IoU) and Generalized-IoU (GIoU)** is the most commonly used family of similarity measures between two arbitrary shapes. IoU encodes the shape properties of the objects under comparison in the regions they occupy, and captures their similarity by a normalized measure based on the areas (or volumes) of these regions. This construction makes IoU scale-invariant, and hence the defacto base-similarity measure of many performance criteria. However, IoU is insensitive to the shape and proximity of non-overlapping shapes. To this end, a generalization that covers non-overlapping shapes, namely Generalized IoU (GIoU), was proposed in [43].

**Performance evaluations for object detection and instance-level segmentation** consider the similarity/dissimilarity between two sets of shapes, namely the reference (or truth) and predicted sets of bounding boxes or masks. Many popular performance criteria are based on the notion of *true positives* of the prediction set, which are determined by matching predictions with references such that the IoU (or GIoU) value between them is larger than a specified threshold, *e.g.* 0.5 is used in many benchmarks [15, 19, 20]. Note that, the subset of true positives is dependent on choice of thresholds. The (subset of) *false positives* is then defined to be the prediction set excluding all true positives. Similarly, the (subset of) *false negatives* (or misses) is the truth set excluding all true positives.

*F1-score* [7] is one of the most commonly used similarity measure for object detections, where the predictions are sets of bounding box coordinates with no confidence scores nor category labels, *e.g.* salient object detection [7]. F-measure captures the similarity with the harmonic mean of precision (the ratio of true positives to predictions) and recall (the ratio of true positives to truths).

*Average Precision (AP) and mean AP (mAP)* [19, 39] are perhaps the most popular performance criteria for single-category and multi-category label object detection/instance-segmentation, respectively. When predictions include confidence scores, true positives are determined by a non-optimal greedy assignment strategy that matches (with references) those with higher confidence scores first [19, 39]. Precision and recall can be expressed as a curve generated from different confidence threshold values. AP approximates the area under the precision-recall curve by interpolating precision samples in different recalls values [19]. For multi-category label predictions, the mean AP (mAP) over all categories is used. Note that ranking the predictions via these criteria can be sensitive to the choice of IoU (GIoU) thresholds. For this reason the MS COCO Benchmark challenge [39] averages

mAP across multiple IoU thresholds.

*Log-average miss rate (log-AMR)* [17] is another popular performance criterion for object detection. Given the matches between references and predictions as per AP, the miss rate is plotted against the false positives per image (FPPI) rate. Similar to AP, Log-AMR approximates the area under the miss rate versus FPPI curve from a finite number of samples.

**Performance evaluations for multi-object tracking** consider the similarity/dissimilarity between sets of reference and predicted tracks. Performance criteria usually rely on IoU or Euclidean distance to match reference tracks with predicted tracks, at each time step [5], or on the entire duration [44]. Other performance criteria such as trajectories-based measures [37], configuration distance and purity measure [53], or global mismatch error [3] were also developed based on similar constructions. Hence, we consider the following two most widely used criteria.

*Multi-Object Tracking Accuracy (MOTA)* [5] is based on pairing, at each frame, reference objects and predicted objects with separation distances below a threshold. From this pairing the mismatch error that captures label inconsistency is the total number of times that track identities are switched. The MOTA score is defined as one minus the normalized (by the total number of reference tracks) sum of mismatch error, and the total number (over all frames) of false positives and false negatives.

*IDF1* [44] is based on pairing reference tracks to predicted tracks so as to minimize the sum of, false positives and false negatives from each pair, for a given distance/IoU threshold. Dummy trajectories are used to account for the cardinality mismatch between the reference and predicted sets. From the optimal pairing, the IDPrecision, IDRecall, and subsequently IDF1 scores are given by the total number of false positives and false negatives of the pairs.

## 3. Guidelines for Selection of Performance Criteria

A performance criterion quantifies (by a numerical value) the similarity/dissimilarity of the output of an algorithm to a nominal reference. For basic vision tasks, this can be done in many ways, from hand-crafted measures based on intuition to using actual human assessments, each with its own merits and drawbacks. Regardless of its conception, the fundamental question is: how can we trust that a performance criterion does what we expect it to do, *i.e.* is it trustworthy?

In this section we attempt to answer the above question by suggesting guidelines for certifying trustworthiness of criteria based on the notions of mathematical consistency, meaningfulness, and reliability. We discuss the meaning and rationale behind these concepts, which are necessary for validating trustworthiness of existing or new criteria. Contrary

to prevailing belief, we show that the well-known performance criteria discussed in Section 2 are not mathematically consistent.

**(i) Mathematical Consistency:** Mathematical considerations are critical in ensuring trustworthiness of performance criteria. Relying purely on intuitive indicators is not adequate for rigorous scientific performance valuation. This is especially true in basic vision problems, where *ground truths* are not available (except for simulated data) and only *approximate truths* (acquired through some measurement processes, *e.g.* manual annotation which is rather subjective) can be used. In this case a performance criterion only captures the similarity/dissimilarity between the predictions and approximate truths. It is implicitly assumed that the similarity/dissimilarity measure is *mathematically consistent* in the following sense: suppose that the approximate truth is “close” (*i.e.* highly similar) to the ground truth, then being “close” to the approximate truth means being “close” to the ground truth. However, this assumption does not necessarily hold even for similarity/dissimilarity between two shapes, let alone two sets of shapes, as illustrated in Fig. 1.

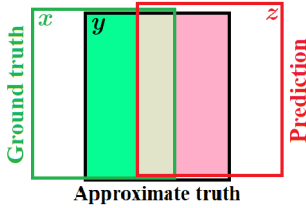


Figure 1: For an IoU threshold of 0.5, the Prediction is “closest” to the Approximate truth ( $F1 = 1$ ), which is “closest” to Ground truth ( $F1 = 1$ ). Thus, the Prediction is expected to be similar to the Ground truth, but they have zero  $F1$  similarity score.

According to the  $F1$  criteria, even though the prediction is “closest” (indicated by the best  $F1$  score) to the approximate truth, which in turn is “closest” to the ground truth, it bears no similarity with the ground truth whatsoever (zero  $F1$  score).

Mathematical consistency is fundamental to performance evaluation, and the above example demonstrates that it cannot be taken for granted. One way to ensure mathematical consistency is to consider (*mathematical*) *metrics*—dissimilarity measures with certain mathematical properties. Specifically, a function  $d : \mathcal{S} \times \mathcal{S} \rightarrow [0; \infty)$  is called a metric (or distance function) on the space  $\mathcal{S}$ , if it satisfies:

1. (Identity)  $d(x, y) = 0$  if and only if  $x = y$  ;
2. (Symmetry)  $d(x, y) = d(y, x)$  for all  $x, y \in \mathcal{S}$  ;
3. (Triangle inequality)  $d(x, z) \leq d(x, y) + d(y, z)$  for all  $x, y, z \in \mathcal{S}$ .

The triangle inequality warrants mathematical consistency, *i.e.* if the prediction  $z$  is “close” to the approximate truth  $y$ , and assuming that the approximate truth  $y$  is “close” to the

ground truth  $x$ , then the triangle inequality asserts that the prediction  $z$  is also “close” to the ground truth  $x$ .

Our interest lies not only in the dissimilarity between two shapes, but dissimilarity between two finite sets of shapes. Fulfillment of the metric properties not only ensure mathematical consistency but also allow us to make use of the substantial body of knowledge on metrics. Metrics are also important in machine learning problems for sets of shapes. The fundamental result that enables the Neural-Net universal approximation of input-to-output mappings, requires the mappings to be continuous [13, 27]. When the input and/or outputs are sets of shapes, metrics provide the notion of continuity needed for Neural-Net universal approximation. In statistical learning, metrics provide the notion of convergence required for statistical consistency of estimates/predictions. Similarly, in numerical optimization, it allows us to convey the notion of how iterates of an algorithm approach a local/global solution. Hence, we advocate metric properties for basic vision performance criteria.

**Remark:** All criteria discussed in Section 2 are not mathematically consistent because they rely on thresholding the base-similarity/dissimilarity to determine the number of true positives (that solely define the criteria). Mathematical consistency of a criterion can be examined by considering the metric properties of its equivalent dissimilarity measure  $d$ , obtained via monotonically re-mapping the criterion’s range into  $[0; \infty)$  with  $d(X, X) = 0$ . The following 1-D counter example, along the lines of that in Fig. 1, shows that all these criteria violate the *Triangle Inequality*.

Let  $\{x\}$  and  $\{y\}$  denote the reference set and prediction set (for multi-object tracking  $x$  and  $y$  would represent unit-length tracks). Given a threshold  $\theta > 0$ , the number of true positives is given by the indicator function  $\mathbf{1}(|x - y| \leq \theta)$  (which equals 1 if  $|x - y| \leq \theta$ , and 0 otherwise). Despite differences amongst the criteria in Section 2, we can abstract that any dissimilarity measure  $d(\{x\}, \{y\})$  of a criterion is a function of only  $\mathbf{1}(|x - y| \leq \theta)$ , since number of false positives and false negatives also depend on this. More concisely,  $d(\{x\}, \{y\}) = D(\mathbf{1}(|x - y| \leq \theta))$ , where is  $D$  a function such that:  $D(1) = 0$  (because  $d(\{x\}, \{x\}) = 0$  and  $d(\{x\}, \{x\}) = D(1)$ ); and  $D(0) > 0$  (because if  $D(0) = 0$ , then  $d(\{x\}, \{y\}) = 0$ , for all  $x, y$ , making this a trivial criterion). Now, the dissimilarity measure  $d$  violates the *Triangle Inequality* because  $d(\{x - 0.6\theta\}, \{x + 0.6\theta\}) = D(0) > 0$ , but  $d(\{x - 0.6\theta\}, \{x\}) + d(\{x\}, \{x + 0.6\theta\}) = D(1) + D(1) = 0$ . It also violates the *Identity* property because  $d(\{x\}, \{x + 0.6\theta\}) = D(1) = 0$ . Section A of the appendix shows individual examples.

**(ii) Meaningfulness:** Mathematical consistency alone is not sufficient to warrant meaningful performance evaluation. Consider the simple sanity check for (multi-object) detection on the unit-diameter disc in Fig. 2. In scenario (i) the detector achieves 0.02 accuracy for all 100 points, while in

(ii) it is off by 0.6 even with only one point. Unequivocally, the prediction error–dissimilarity between the prediction and ground truth sets—in scenario (i) is smaller than that in (ii), *i.e.* performance in (i) is better than that in (ii). A naive metric such as the minimum sum of dislocation errors is mathematically consistent, but proclaims the performance in (ii) to be better than that in (i), which is nonsensical. In contrast, a criterion like F1 is more meaningful, confirming (for a 0.5 threshold) better performance in (i) than in (ii), and even if the threshold is varied, would never declare (ii) to be the better.

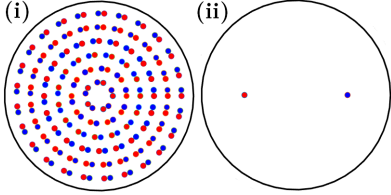


Figure 2: Scenario (i) 100 reference points (red) and 100 predicted points (blue), each of which is 0.02 from the nearest reference; scenario (ii) 1 reference point, 1 predicted point separated by 0.6. Minimum-sum-of-errors (dissimilarity) in scenario (i) is 2, but 0.6 in (ii). F1 similarity score (with 0.5 threshold) in scenario (i) is 1, and 0 in (ii).

The example in Fig. 2 motivates the need to verify whether a criterion captures the intent of the performance evaluation exercise. Since this is independent of mathematical consistency, there is no analytical tools at our disposal, and it becomes necessary to consider experimental verification via sanity tests. The idea behind sanity testing is to consider scenarios where it is possible to unequivocally evaluate/rank based on the intent of the evaluation exercise, and verify whether a performance criterion corroborates this intent.

We suggest a systematic approach to performing sanity tests via simulation. Our strategy is to first, generate a number of reference sets, from models based on typical data from the application. Suppose that the sources of errors for the application can be identified, *e.g.* false negatives/positives, location/shape errors, *etc.* We then generate a series of prediction sets with pre-determined performance ranking by perturbing the reference sets with simulated errors. Predictions generated from small perturbations are ranked higher than those generated from large perturbations. This strategy enables the generation of complex scenarios with a combination of error sources, where the pre-determined rankings are not obvious to the human eye. A meaningful performance criterion should be consistent with the pre-determined rankings.

**(iii) Reliability:** The rankings produced by a criterion should not be affected by the choice of hyper-parameters, *e.g.* IoU/GIoU thresholds. Otherwise, it is possible to dubiously promote certain solutions via hyper-parameter tuning.

Mathematical consistency and good performance in sanity tests do not guarantee reliability. Strategies to eliminate hyper-parameters by marginalizing them out (*e.g.* averaging mAP over different IoU thresholds [39]), may lead to even larger ranking discrepancies for criteria with higher hyper-parameter sensitivity, as indicated by our experiments. Hence, reliable criteria should be insensitive to variations of their hyper-parameters.

**Assessing the performance criteria** themselves is needed to validate meaningfulness/reliability in sanity tests. Such assessment can be accomplished by measuring the *ranking errors* committed by the criteria against the pre-determined ranking. Given a ranking for  $K$  prediction sets, we call the tuple containing the rank of each prediction set the *ranking vector*. Noting that the ranking error should take into account the magnitude of the incorrect ranks, the Manhattan distance between the true ranking vector and the criterion’s ranking vector, succinctly captures the ranking error.

#### 4. Metrics: Alternative Performance Evaluation Criteria

In this section we explore (mathematical) metrics or distances between two sets of shapes as mathematically consistent alternative performance criteria for basic vision tasks. This is accomplished by composing distances between two sets of points with distances between two shapes.

**4.1. Metrics for Shapes:** For any two arbitrary shapes  $x, y$ , the Intersection over Union (IoU) similarity index is given by  $IoU(x, y) = |x \cap y| / |x \cup y| \in [0; 1]$ , where  $|\cdot|$  denotes hyper-volume. For convex shapes, the Generalized IoU index is given by  $GIoU(x, y) = IoU(x, y) - |C(x \cup y) \setminus (x \cup y)| / |C(x \cup y)|$ , where  $C(x \cup y)$  is the convex hull of  $x \cup y$  [43]. Note that unlike  $IoU(x, y)$ ,  $GIoU(x, y) \in [-1; 1]$ . For arbitrary shapes, the definition of GIoU is given in the supplementary section of [43]. As the defacto base-similarity measure for many performance criteria, IoU/GIoU is a natural candidate for base-distances between shapes, required to construct distances between sets of shapes. The metric forms of IoU and GIoU, respectively are  $d_{IoU}(x, y) = 1 - IoU(x, y)$  and  $d_{GIoU}(x, y) = \frac{1 - GIoU(x, y)}{2}$  [43], which are indeed metrics bounded by one.

The IoU/GIoU distance can also be extended to accommodate basic vision solutions that attach to each shape a confidence score. Note that such scores can be normalized to the interval  $(0, 1]$  since reference shapes have maximum confidence scores of one. To determine the IoU/GIoU distance between shapes with confidence scores, we take the Cartesian products of the shapes with their corresponding confidence scores to form augmented shapes in a higher dimensional space, and then compute the IoU/GIoU distance between these augmented shapes. This strategy can



be applied to improve mAP and log-AMR performance via optimal assignment (see Section C.1 of the appendix).

**4.2. Metrics for Sets of Shapes:** Our interest lies in the distance between two point patterns or finite subsets of a metric space  $(\mathbb{W}, \underline{d})$ , where  $\underline{d} : \mathbb{W} \times \mathbb{W} \rightarrow [0; 1]$  denotes the *base-distance* between the elements of  $\mathbb{W}$ . More specifically,  $\mathbb{W}$  is the space of arbitrary/convex shapes and  $\underline{d}$  is the IoU/GIoU distance. This metric space can be visualized as the unit-diameter disc, see e.g. Fig. 2.

One option is to consider classical set distances such as *Hausdorff* and *Wasserstein* [16, 21, 26] (e.g. Earth mover’s distance [45]). These metrics are, respectively, constructed for arbitrary sets and probability distributions (see the appendix, Section C.2 for details). Thus, whether they are meaningful—capturing such intent—in the context basic vision problems, remain to be verified.

The intent behind the performance evaluation criteria discussed in Section 2 is to capture the dislocation and cardinality error. What these criteria have in common is the pairing of predicted and reference points so as to minimize the sum of base-distances between the pairs, either by greedy assignment or optimal assignment. Despite differences amongst various criteria, the dislocation is determined from the matched pairs (those with base-distances below a threshold), and the cardinality error from unmatched elements, which are then combined to produce a normalized or averaged score.

An alternative to classical set distances is to find a metric that captures the above intent. Instead of thresholding the base-distance between the pairs to determine true positives, which violates the metric properties, we can capture the same intent simply by adding the minimum sum of base-distances (representing dislocation) with the number of unpaired elements (representing cardinality error), and normalize by the total number of pairs and unpaired elements. Simply put, this is the best-case per-object dislocation and cardinality error, i.e. for  $X = \{x_1, \dots, x_m\}$  and  $Y = \{y_1, \dots, y_n\}$ ,

$$d_0(X, Y) = \frac{1}{n} \left( \min_{\pi \in \Pi_n} \sum_{i=1}^m \underline{d}(x_i, y_{\pi(i)}) + (n - m) \right), \quad (1)$$

if  $n \geq m > 0$ , where  $\Pi_n$  is the set of all permutations of  $\{1, 2, \dots, n\}$ , additionally:  $d_0(X, Y) = d_0(Y, X)$ , if  $m > n > 0$ ;  $d_0(X, Y) = 1$ , if one of the set is empty; and  $d_0(\emptyset, \emptyset) = 0$ . This normalized error is indeed a metric, specifically, an *Optimal Sub-Pattern Assignment (OSPA)* metric [49].

**4.3. Metrics for Sets of Tracks:** For performance evaluation of multi-object tracking, the metrics for sets of shapes discussed earlier are not directly applicable because a track cannot be treated as a shape or a set of shapes due to the temporal ordering of its constituents. A *track* in the metric space  $(\mathbb{W}, \underline{d})$  and discrete-time window  $\mathbb{T}$ , is defined as a

mapping  $f : \mathbb{T} \mapsto \mathbb{W}$ . Its *domain*  $\mathcal{D}_f \subseteq \mathbb{T}$ , is the set of time instants when the object/track has a state in  $\mathbb{W}$ . This definition accommodates the so-called fragmented tracks, i.e. tracks with domains that are not intervals.

A meaningful distance between two sets of tracks requires a meaningful base-distance between two tracks. There are various ways to construct such base-distances. The most suitable is a time-averaged OSPA distance between two tracks  $f$  and  $g$  over instants when at least one of the tracks exists, i.e.

$$\tilde{d}(f, g) = \sum_{t \in \mathcal{D}_f \cup \mathcal{D}_g} \frac{d_0(\{f(t)\}, \{g(t)\})}{|\mathcal{D}_f \cup \mathcal{D}_g|}, \quad (2)$$

if  $\mathcal{D}_f \cup \mathcal{D}_g \neq \emptyset$ , and  $\tilde{d}(f, g) = 0$ , if  $\mathcal{D}_f \cup \mathcal{D}_g = \emptyset$ . Note that  $\tilde{d}$  is bounded by 1, and is indeed a metric as shown in [2]. Using the Hausdorff, Wasserstein, and OSPA metrics, respectively, with base-distance  $\underline{d}$ , yield the Hausdorff( $\underline{d}$ ), Wasserstein( $\underline{d}$ ), and OSPA( $\underline{d}$ ) distances between two sets of tracks. The latter is called OSPA<sup>(2)</sup> (since  $\tilde{d}$  is constructed from OSPA) and can be interpreted as the time-averaged per-track error, which takes into account errors in localisation, cardinality, track fragmentation and track identity switching [2]. A dropped track that later regained with the same identity, yields a smaller penalty than if it were regained with a different identity.

**Remark:** The Hausdorff, Wasserstein, and OSPA metrics (with both base-distances  $\underline{d}$  and  $\tilde{d}$ ) discussed above are mathematically consistent (by default) and reliable (no hyper-parameters), but whether they are meaningful or not will be examined in Section 5. Nonetheless, they pass the sanity test of Fig. 2, with all three agreeing on distances of 0.02 and 0.6 for scenarios (i) and (ii), respectively. Similar to popular criteria in the literature, normalization is important, without it OSPA is obviously still a metric (the naive metric that fails the sanity test of Fig. 2) albeit no longer meaningful. Further discussions on these metrics are given in Section C.2 of the appendix.

## 5. Experimental results

**5.1. Evaluation Results on Sanity Tests:** This experiment examines, via sanity tests, the behaviours of different performance criteria for bounding box multi-class multi-object detection, and single-class multi-object tracking. Tests on instance-level segmentation masks are omitted as bounding boxes can be interpreted as masks, with both having similar properties in terms of similarity measure. The detection experiments without class and confidence score for comparison with F1-score is provided in the appendix (Section D.2.2) for completeness. The construction of the tests are briefly described in the following, further details can be found in Section D.2 of the appendix.

**Multi-Class Multi-Object Detection:** We first sample a set of bounding boxes for the reference set, and then perturb this set to form 20 prediction sets with pre-determined

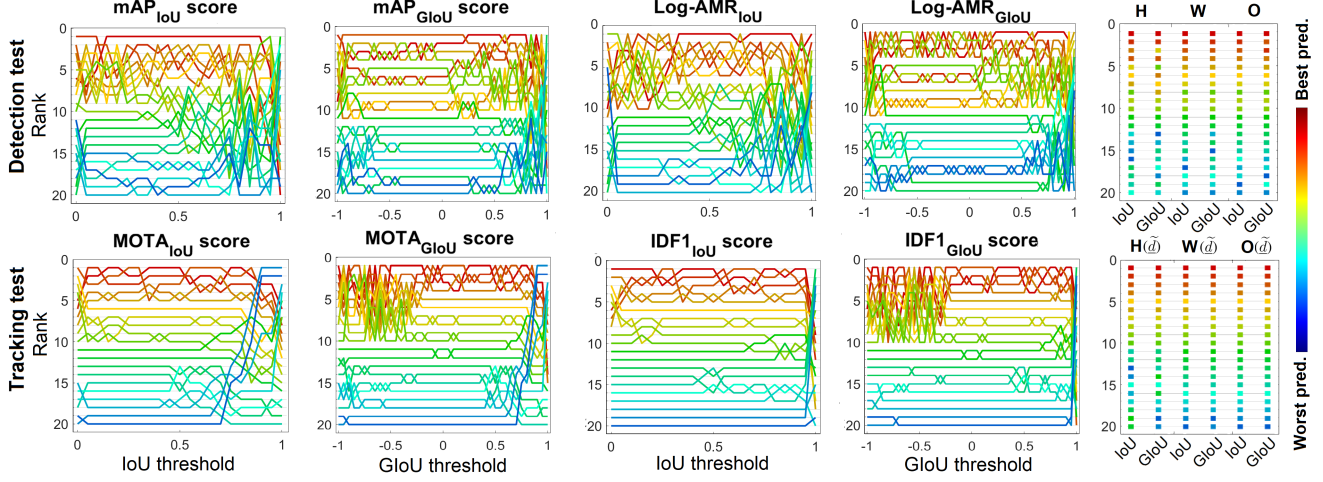


Figure 3: Ranks of prediction sets (for a sample reference set) according to various traditional criteria over a range of IoU/GIoU thresholds, and according to Hausdorff (H), Wasserstein (W), and OSPA (O) metrics. The pre-determined ranks are color-coded from worst (blue) to best (red).

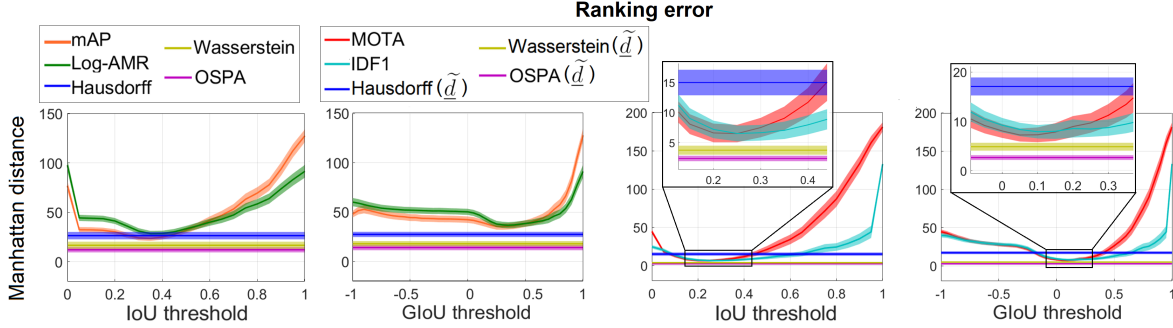


Figure 4: Mean Manhattan ranking errors (from the true ranking) of various criteria at different thresholds, over all Monte Carlo trials in **detection test** (two plots on the left) and **tracking test** (two plots on the right). Shaded area around each curve indicates 0.2-sigma bound.

ranks. The lower the prediction set is ranked: the higher the disturbance in locations and sizes, the higher the number of missed objects, false positives, and predictions with incorrect classes; and the lower the detection confidence scores for predicted objects with correct class. The evaluation score/rate/distance is averaged across all classes.

**Multi-Object Tracking:** First, we simulate the initial states of the tracks by generating a random number of random bounding boxes at random instances in the 100 time-step window. We then simulate the track lengths randomly from the interval  $\{50, \dots, 100\}$  and, accordingly, propagate the initial states in time via the constant velocity model to simulate a reference set (of tracks). We generate 20 predictions sets (of tracks) with pre-determined ranks by perturbing the reference set. The simulated numbers of missed objects at each time step and false tracks increase from the best prediction set to the worst. Simulated false tracks also exhibit constant velocity motion during their active periods while their sizes vary randomly. Identities swapping events are simulated so that the lower rank prediction sets have, at the

same level of mutual IoU, more tracks identity swapping.

**Results and discussion:** Fig. 3 shows traditional performance criteria producing unreliable ranking with the ranks switching severely across different IoU/GIoU thresholds. In general, more meaningful criteria should incur smaller ranking errors. To assess the meaningfulness of a criterion, we generate 100 reference sets, and for each reference set we repeat the experiment (*i.e.* perturb it to simulate 20 prediction sets) 100 times to compute the average Manhattan ranking error. Fig. 4 further confirms that the ranking accuracy (meaningfulness) of these criteria also vary considerably across the range of IoU/GIoU thresholds, albeit generally better at low thresholds. Tab. 1, shows that marginalizing the hyper-parameters may produce: less meaningful ranking compared to the optimal threshold in the detection test (see mAP score with IoU); and severe mis-ranking in the tracking test. One explanation is that the ranking accuracy of the traditional criteria heavily depend on the threshold values, and averaging over a fixed range of thresholds may distort the criteria’s original intent (and meaningfulness). At their optimal

Table 1: Means (and standard deviations) of Manhattan ranking errors of various criteria at certain thresholds, over all Monte Carlo trials. The subscripts of IoU/GIoU indicate the threshold values; "optimal" threshold is the one with best ranking accuracy; "M" threshold indicates that the evaluation is done via averaging the score/rate over the range 0.5 to 0.95 in steps of 0.05.

Multi-object detection test						
	IoU <sub>0.5</sub>	IoU <sub>optimal</sub>	IoU <sub>M</sub>	GIoU <sub>0</sub>	GIoU <sub>optimal</sub>	GIoU <sub>M</sub>
mAP	31.8 (14.7)	23.6 (12.6)	26.2 (13.6)	42.6 (16.6)	35.54 (16.1)	32.3 (15.3)
Log-AMR	33.2 (14.9)	28.4 (14.1)	27.43 (13.0)	50.3 (15.4)	36.85 (15.6)	31.6 (13.3)
Hausdorff		26.3 (18.2)			27.6 (13.3)	
Wasserstein		16.7 (18.2)			18.1 (13.0)	
OSPA		<b>12.1 (13.2)</b>			<b>14.3 (13.4)</b>	
Multi-object tracking test						
MOTA	21.2 (22.8)	6.6 (7.3)	55.0 (40.4)	8.0 (6.9)	7.2 (6.5)	60.5 (42.3)
IDF1	10.4 (10.6)	6.5 (6.5)	10.1 (11.1)	9.2 (7.3)	7.9 (6.8)	12.0 (13.1)
Hausdorff( $\tilde{d}$ )		15.0 (10.6)			17.1 (9.1)	
Wasserstein( $\tilde{d}$ )		3.8 (3.7)			4.8 (4.0)	
OSPA( $\tilde{d}$ )		<b>2.8 (2.3)</b>			<b>2.6 (2.4)</b>	

thresholds (which are not available in practice), traditional criteria produce relatively more accurate ranking than the Hausdorff metric but less accurate than those of Wasserstein and OSPA, with the latter being the most accurate. This can be attributed to the better sensitivities of the Wasserstein and OSPA metrics to both dislocation and cardinality error. Moreover, the OSPA metric explicitly captures these errors with the same intuitive intent as the traditional criteria, and hence more meaningful than Wasserstein.

**5.2. Evaluation on Real Benchmark Dataset:** We now show how the existing performance criteria and suggested metrics rank state-of-the-art detectors and trackers on real benchmark dataset.

**COCO 2017 validation set:** For bounding box detection, we use different detection models including the Faster-RCNN [42], Single Shot Detector (SSD) [40] and the Regional based Fully Convolutional Networks (RFCN) [14] with different backbones (Inception Network [56, 57], Residual Network (ResNet) [23], Inception ResNet [55] with atrous pooling strategy [10], Neural Architecture Search (NAS) [60], Mobilenets [28], Mobilenets v2 [48], Feature Pyramid Network (FPN) [38] and Pooling Pyramid Network (PPN) [29]) to detect objects. For instance-level segmentation, we use the Mask-RCNN [22] model with different network structures (FPN, ResNet, Inception ResNet) and ResNext model [58] (with FPN) to produce predictions. GIoU-based criteria are not available in Fig. 5 (ii) because the computation of GIoU for arbitrary masks are not yet available [43].

**MOTChallenge (MOT17) dataset:** This experiment ranks predictions from 21 trackers [1, 4, 6, 8, 9, 11, 18, 24, 25, 30, 31, 33, 35, 36, 46, 47, 50–52, 54, 59] on the MOT17 [41]

leaderboard, according to various criteria. The tracking results are obtained by applying the trackers to track human in 7 training sequences and each with 3 detection methods.

**Results and discussion:** Fig. 5 shows that the ranks vary across different traditional criteria, albeit mAP and log-AMR (at a 0.5 IoU threshold) produce similar ranks due to their similar constructions. The metrics rankings tends to be similar to each other, but quite different from those of the traditional criteria. For example, "Mask RCNN Inception v2" in plot (ii) performs really well according to the mAP and log-AMR criteria (with 0.5 IoU threshold), but poorly according to the mAP COCO criteria and metrics criteria. Ranks from the same metric do not seem to vary significantly from IoU to GIoU base-distances. Further details on the behaviour of traditional criteria over different IoU/GIoU thresholds are given in the appendix (Section D.4).

## 6. Conclusions

We have formulated the notion of trustworthiness for performance evaluation criteria in basic vision problems via mathematical consistency, meaningfulness and reliability. We also suggested metrics for sets of shapes as mathematically consistent and reliable alternatives over the (neither mathematically consistent nor reliable) traditional performance criteria. Empirically, metrics do not necessarily yield more meaningful rankings than some of the popular criteria. Nonetheless, metrics that capture the intuition behind these criteria yield more meaningful rankings, and hence more trustworthy. While our study is by no means comprehensive, we hope it paves the way towards a richer and versatile set of performance evaluation tools for computer vision.

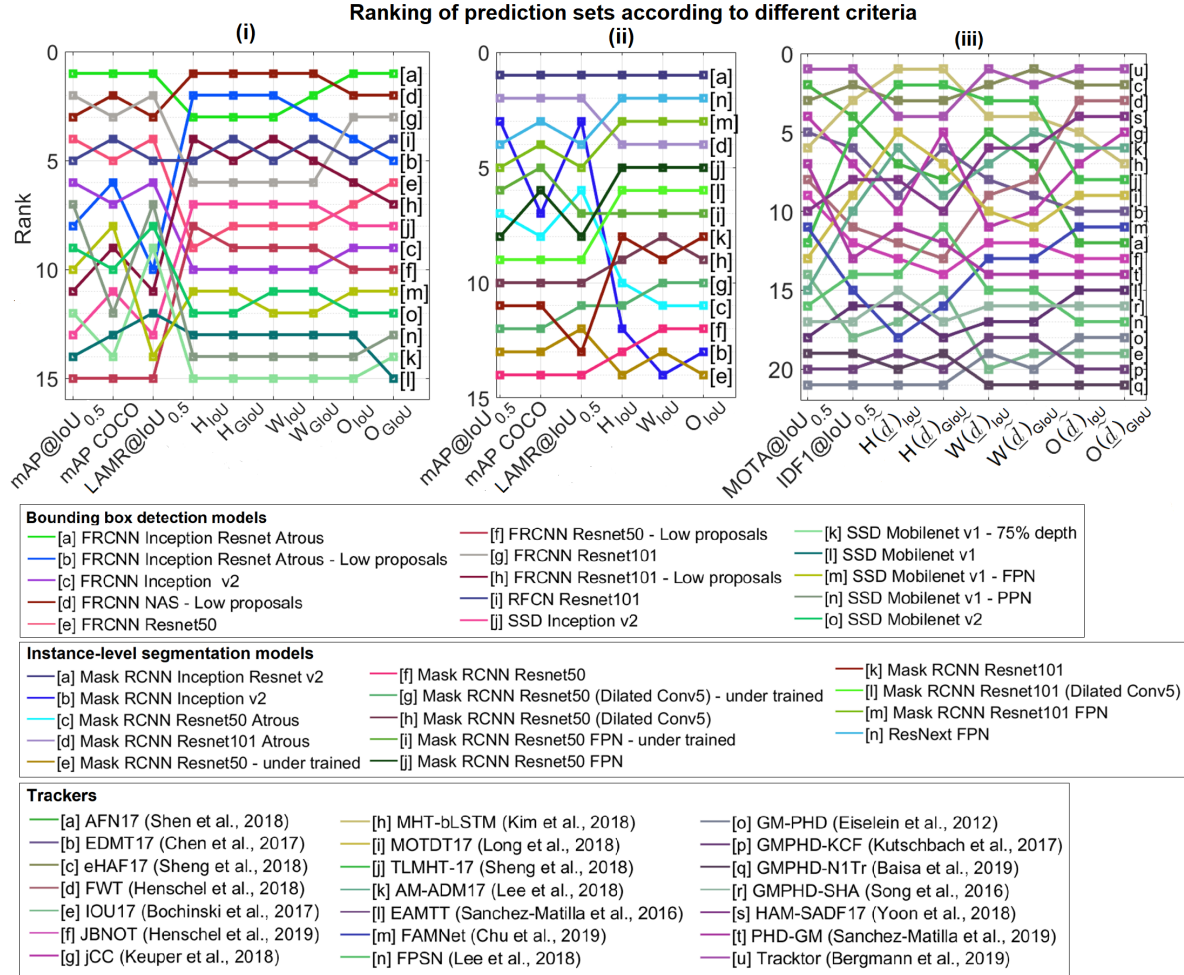


Figure 5: Ranks, according various criteria, of predictions in (i) COCO bounding box detection, (ii) COCO instance-level segmentation and (iii) MOTChallenge tracking. **mAP COCO**: averaged mAP over IoU threshold of 0.5 to 0.95 in steps of 0.05. **LAMR**: Log-AMR. **H**: Hausdorff. **W**: Wasserstein. **O**: OSPA.



## References

- [1] N. L. Baisa and A. Wallace. Development of a n-type gm-phd filter for multiple target, multiple type visual tracking. *Journal of Visual Communication and Image Representation*, 59:257 – 271, 2019.
- [2] M. Beard, B.-T. Vo, and B.-N. Vo. A solution for large-scale multi-object tracking. *IEEE Transactions on Signal Processing*, 68:2754–2769, 2020.
- [3] H. Ben Shitrit, J. Berclaz, F. Fleuret, and P. Fua. Tracking multiple people under global appearance constraints. In *International Conference on Computer Vision (ICCV)*, 2011.
- [4] P. Bergmann, T. Meinhardt, and L. Leal-Taixé. Tracking without bells and whistles. In *International Conference on Computer Vision (ICCV)*, 2019.
- [5] K. Bernardin and R. Stiefelhagen. Evaluating multiple object tracking performance: The clear mot metrics. *Journal on Image and Video Processing*, 2008:1, 2008.
- [6] E. Bochinski, V. Eiselein, and T. Sikora. High-speed tracking-by-detection without using image information. In *International Conference on Advanced Video Signal-based Surveillance (AVSS)*, 2017.
- [7] A. Borji, M.-M. Cheng, H. Jiang, and J. Li. Salient object detection: A benchmark. *IEEE Transactions on Image Processing*, 24(12):5706–5722, 2015.
- [8] J. Chen, H. Sheng, Y. Zhang, and Z. Xiong. Enhancing detection model for multiple hypothesis tracking. In *Conference on Computer Vision and Pattern Recognition (CVPR)*, 2017.
- [9] L. Chen, H. Ai, Z. Zhuang, and C. Shang. Real-time multiple people tracking with deeply learned candidate selection and person re-identification. In *International Conference on Multimedia and Expo (ICME)*, 2018.
- [10] L. Chen, G. Papandreou, I. Kokkinos, K. Murphy, and A. L. Yuille. Deeplab: Semantic image segmentation with deep convolutional nets, atrous convolution, and fully connected crfs. *IEEE Transactions on Pattern Analysis and Machine Intelligence*, 40(4):834–848, 2018.
- [11] P. Chu and H. Ling. Famnet: Joint learning of feature, affinity and multi-dimensional assignment for online multiple object tracking. In *International Conference on Computer Vision (ICCV)*, 2019.
- [12] M. Cordts, M. Omran, S. Ramos, T. Rehfeld, M. Enzweiler, R. Benenson, U. Franke, S. Roth, and B. Schiele. The cityscapes dataset for semantic urban scene understanding. In *Conference on Computer Vision and Pattern Recognition (CVPR)*, 2016.
- [13] G. Cybenko. Approximation by superpositions of a sigmoidal function. *Mathematics of Control, Signals, and Systems*, 2(4):303–314, 1989.
- [14] J. Dai, Y. Li, K. He, and J. Sun. R-fcn: Object detection via region-based fully convolutional networks. In *Conference on Neural Information Processing Systems (NeurIPS)*, 2016.
- [15] P. Dendorfer, H. Rezatofighi, A. Milan, J. Shi, D. Cremers, I. Reid, S. Roth, K. Schindler, and L. Leal-Taixé. Cvpr19 tracking and detection challenge: How crowded can it get? *arXiv e-prints*, page arXiv:1906.04567, 2019.
- [16] R. L. Dobrushin. Prescribing a system of random variables by conditional distributions. *Theory of Probability & Its Applications*, 15(3):458–486, 1970.
- [17] P. Dollar, C. Wojek, B. Schiele, and P. Perona. Pedestrian detection: An evaluation of the state of the art. *IEEE Transactions on Pattern Analysis and Machine Intelligence*, 34(4):743–761, 2011.
- [18] V. Eiselein, D. Arp, M. Pätzold, and T. Sikora. Real-time multi-human tracking using a probability hypothesis density filter and multiple detectors. In *International Conference on Advanced Video Signal-based Surveillance (AVSS)*, 2012.
- [19] M. Everingham, L. Van Gool, C. Williams, J. Winn, and A. Zisserman. The pascal visual object classes (voc) challenge. *International Journal of Computer Vision*, 88(2):303–338, 2010.
- [20] A. Geiger, P. Lenz, and R. Urtasun. Are we ready for autonomous driving? The KITTI Vision Benchmark Suite. In *Conference on Computer Vision and Pattern Recognition (CVPR)*, 2012.
- [21] B. Grunbaum. *Convex polytopes*. Interscience, 1967.
- [22] K. He, G. Gkioxari, P. Dollár, and R. Girshick. Mask r-cnn. In *International Conference on Computer Vision (ICCV)*, 2017.
- [23] K. He, X. Zhang, S. Ren, and J. Sun. Deep residual learning for image recognition. In *Conference on Computer Vision and Pattern Recognition (CVPR)*, 2016.
- [24] R. Henschel, L. Leal-Taixé, D. Cremers, and B. Rosenhahn. Fusion of head and full-body detectors for multi-object tracking. In *Conference on Computer Vision and Pattern Recognition (CVPR)*, 2018.
- [25] R. Henschel, Y. Zou, and B. Rosenhahn. Multiple people tracking using body and joint detections. In *Conference on Computer Vision and Pattern Recognition (CVPR)*, 2019.
- [26] J. R. Hoffman and R. P. S. Mahler. Multitarget miss distance via optimal assignment. *IEEE Transactions on Systems, Man, and Cybernetics - Part A: Systems and Humans*, 34(3):327–336, 2004.
- [27] K. Hornik. Approximation capabilities of multilayer feedforward networks. *Neural Networks*, 4(2):251 – 257, 1991.

- [28] A. G. Howard, M. Zhu, B. Chen, D. Kalenichenko, W. Wang, T. Weyand, M. Andreetto, and H. Adam. Mobilenets: Efficient convolutional neural networks for mobile vision applications. *arXiv e-prints*, page arXiv:1704.04861, 2017.
- [29] P. Jin, V. Rathod, and X. Zhu. Pooling pyramid network for object detection. *arXiv e-prints*, page arXiv:1807.03284, 2018.
- [30] M. Keuper, S. Tang, B. Andres, T. Brox, and B. Schiele. Motion segmentation multiple object tracking by correlation co-clustering. *IEEE Transactions on Pattern Analysis and Machine Intelligence*, 42(1):140–153, 2020.
- [31] C. Kim, F. Li, and J. M. Rehg. Multi-object tracking with neural gating using bilinear lstm. In *European Conference on Computer Vision (ECCV)*, 2018.
- [32] A. Kirillov, K. He, R. Girshick, C. Rother, and P. Dollár. Panoptic segmentation. In *Conference on Computer Vision and Pattern Recognition (CVPR)*, 2019.
- [33] T. Kutschbach, E. Bochinski, V. Eiselein, and T. Sikora. Sequential sensor fusion combining probability hypothesis density and kernelized correlation filters for multi-object tracking in video data. In *International Conference on Advanced Video Signal-based Surveillance (AVSS)*, 2017.
- [34] L. Leal-Taixé, A. Milan, I. Reid, S. Roth, and K. Schindler. MOTChallenge 2015: Towards a benchmark for multi-target tracking. *arXiv e-prints*, page arXiv:1504.01942, 2015.
- [35] S. Lee and E. Kim. Multiple object tracking via feature pyramid siamese networks. *IEEE Access*, 7:8181–8194, 2019.
- [36] S. Lee, M. Kim, and S. Bae. Learning discriminative appearance models for online multi-object tracking with appearance discriminability measures. *IEEE Access*, 6:67316–67328, 2018.
- [37] Y. Li, C. Huang, and R. Nevatia. Learning to associate: Hybridboosted multi-target tracker for crowded scene. In *Conference on Computer Vision and Pattern Recognition (CVPR)*, 2009.
- [38] T. Lin, P. Dollár, R. Girshick, K. He, B. Hariharan, and S. Belongie. Feature pyramid networks for object detection. In *Conference on Computer Vision and Pattern Recognition (CVPR)*, 2017.
- [39] T.-Y. Lin, M. Maire, S. Belongie, J. Hays, P. Perona, D. Ramanan, P. Dollar, and C. L. Zitnick. Microsoft coco: Common objects in context. In *European Conference on Computer Vision (ECCV)*, 2014.
- [40] W. Liu, D. Anguelov, D. Erhan, C. Szegedy, S. Reed, C.-Y. Fu, and A. C. Berg. Ssd: Single shot multibox detector. *Lecture Notes in Computer Science*, pages 21–37, 2016.
- [41] A. Milan, L. Leal-Taixe, I. Reid, S. Roth, and K. Schindler. MOT16: A Benchmark for Multi-Object Tracking. *arXiv e-prints*, page arXiv:1603.00831, 2016.
- [42] S. Ren, K. He, R. Girshick, and J. Sun. Faster r-cnn: Towards real-time object detection with region proposal networks. *IEEE Transactions on Pattern Analysis and Machine Intelligence*, 39(6):1137–1149, 2017.
- [43] H. Rezatofighi, N. Tsoi, J. Gwak, A. Sadeghian, I. Reid, and S. Savarese. Generalized intersection over union: A metric and a loss for bounding box regression. In *Conference on Computer Vision and Pattern Recognition (CVPR)*, 2019.
- [44] E. Ristani, F. Solera, R. Zou, R. Cucchiara, and C. Tomasi. Performance measures and a data set for multi-target, multi-camera tracking. In *European Conference on Computer Vision (ECCV)*, 2016.
- [45] Y. Rubner, C. Tomasi, and L. J. Guibas. A metric for distributions with applications to image databases. In *International Conference on Computer Vision (ICCV)*, 1998.
- [46] R. Sanchez-Matilla and A. Cavallaro. A predictor of moving objects for first-person vision. In *International Conference on Image Processing (ICIP)*, 2019.
- [47] R. Sanchez-Matilla, F. Poiesi, and A. Cavallaro. Online multi-target tracking with strong and weak detections. In *European Conference on Computer Vision (ECCV)*, 2016.
- [48] M. Sandler, A. Howard, M. Zhu, A. Zhmoginov, and L. Chen. Mobilenetv2: Inverted residuals and linear bottlenecks. In *Conference on Computer Vision and Pattern Recognition (CVPR)*, 2018.
- [49] D. Schuhmacher, B.-T. Vo, and B.-N. Vo. A consistent metric for performance evaluation of multi-object filters. *IEEE Transactions on Signal Processing*, 56(8):3447–3457, 2008.
- [50] H. Shen, L. Huang, C. Huang, and W. Xu. Tracklet association tracker: An end-to-end learning-based association approach for multi-object tracking. *arXiv e-prints*, page arXiv:1808.01562, 2018.
- [51] H. Sheng, J. Chen, Y. Zhang, W. Ke, Z. Xiong, and J. Yu. Iterative multiple hypothesis tracking with tracklet-level association. *IEEE Transactions on Circuits and Systems for Video Technology*, 29(12):3660–3672, 2019.
- [52] H. Sheng, Y. Zhang, J. Chen, Z. Xiong, and J. Zhang. Heterogeneous association graph fusion for target association in multiple object tracking. *IEEE Transactions on Circuits and Systems for Video Technology*, 29(11):3269–3280, 2019.
- [53] K. Smith, D. Gatica-Perez, J. Odobez, and Sileye Ba. Evaluating multi-object tracking. In *Conference on Computer Vision and Pattern Recognition (CVPR)*, 2005.

- [54] Y. Song and M. Jeon. Online multiple object tracking with the hierarchically adopted gm-phd filter using motion and appearance. In *International Conference on Consumer Electronics-Asia (ICCE-Asia)*, 2016.
- [55] C. Szegedy, S. Ioffe, V. Vanhoucke, and A. Alemi. Inception-v4, inception-resnet and the impact of residual connections on learning. In *AAAI Conference on Artificial Intelligence (AAAI)*, 2017.
- [56] C. Szegedy, W. Liu, Y. Jia, P. Sermanet, S. Reed, D. Anguelov, D. Erhan, V. Vanhoucke, and A. Rabinovich. Going deeper with convolutions. In *Conference on Computer Vision and Pattern Recognition (CVPR)*, 2015.
- [57] C. Szegedy, V. Vanhoucke, S. Ioffe, J. Shlens, and Z. Wojna. Rethinking the inception architecture for computer vision. In *Conference on Computer Vision and Pattern Recognition (CVPR)*, 2016.
- [58] S. Xie, R. Girshick, P. Dollár, Z. Tu, and K. He. Aggregated residual transformations for deep neural networks. In *Conference on Computer Vision and Pattern Recognition (CVPR)*, 2017.
- [59] Y. Yoon, A. Boragule, Y. Song, K. Yoon, and M. Jeon. Online multi-object tracking with historical appearance matching and scene adaptive detection filtering. In *International Conference on Advanced Video Signal-based Surveillance (AVSS)*, 2018.
- [60] B. Zoph and Q. V. Le. Neural architecture search with reinforcement learning. In *International Conference on Learning Representations (ICLR)*, 2017.

## APPENDIX

This appendix accompanies the main text and contains further explanations, detailed discussions and additional experiments to support our arguments. Specifically, in Section A, we provide actual formulations of the traditional criteria discussed in the main text together with counter examples to show how the metric properties are violated. In Section B, we elaborate on the construction of sanity tests based on the parameters characterizing the perturbations rather than by visual impression. This section, also provides indicators for ranking consistency (across hyper-parameter values). In Section C, we detail the implementation of the IoU/GIoU extension (proposed in Subsection 4.1 of the main text) used with mAP, log-AMR, in the experiments of Subsection D.5. Section C also provides additional discussions on the point patterns metrics introduced in Subsection 4.2 of the main text. In Section D, we show how the traditional dissimilarity score is affected by the lack of mathematical consistency compared to the (mathematical) metrics. More details on the sanity test experiments in the main text and an extra test on the single-class multi-object detection are also presented in this last section.

### A. On Traditional Performance Criteria

Section 2 of the main text presents traditional criteria based on thresholding to determine the truth-to-prediction matches. These criteria are shown to be mathematically inconsistent via a general 1-D counter example in Section 3(i). In this section, we provide the formulation for each of these criteria and individual counter examples (with bounding boxes).

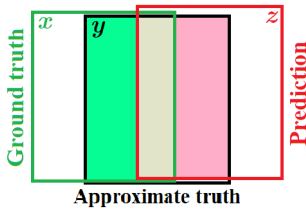


Figure 1: Ground truth, approximate truth and prediction bounding boxes for demonstration of the inconsistency of the traditional criteria.

For a similarity measure  $s$ , we define its corresponding dissimilarity measure between a reference set  $\{x\}$  and a prediction set  $\{y\}$  as  $d_s(\{x\}, \{y\}) = 1 - s(\{x\}, \{y\})$ . For traditional set similarity measures discussed in Section 2 of the main text, this form of dissimilarity measure has the same property as the abstract counterpart defined in the 1-D counter example in last paragraph of Section 3(i). If  $x$  and  $y$  are bounding boxes, the distance  $|x - y|$  can be defined as IoU or GIoU distance (denoted  $d_{IoU}(x, y)$  or  $d_{GIoU}(x, y)$ ).

*F1-score* is a similarity measure which is normalized between 0 and 1. Given the number of false positives as  $FP$ , false negatives as  $FN$  and true positives as  $TP$  the precision ( $P$ ) and recall ( $R$ ) can be calculated respectively as

$$P = \frac{TP}{TP + FP} \text{ and } R = \frac{TP}{TP + FN}.$$

F1 score is then calculated as

$$F1 = 2 \times \frac{P \times R}{P + R}. \quad (1)$$

For the example in Fig. 1, we can assume that there exists a IoU (or GIoU) distance threshold  $\theta$  such that (i) the bounding box  $x$  can be considered as a true positive for the bounding box  $y$  (i.e.  $d_{IoU}(x, y) < \theta$ ), (ii) the bounding box  $y$  can be considered as a true positive for the bounding box  $z$  (i.e.  $d_{IoU}(y, z) < \theta$ ), (iii) but the bounding box  $x$  is a false positive for the bounding box  $z$  (i.e.  $d_{IoU}(x, z) > \theta$ ). Therefore, in both pairs of scenarios  $(x, y)$  and  $(y, z)$ , the precision, recall and consequently F1 score values are equal to one, i.e.  $d_{F1}(\{x\}, \{y\}) = d_{F1}(\{y\}, \{z\}) = 0$ . However, in the pair scenario  $(x, z)$ ,  $P, R$  and consequently  $F1$  values are equal to zero, i.e.  $d_{F1}(\{x\}, \{z\}) = 1$ . Therefore, F1 score, as dissimilarity measure, does not fulfill the following metric properties:

- (Identity)  $d_{F1}(\{x\}, \{y\}) = d_{F1}(\{y\}, \{z\}) = 0$ , but  $x \neq y \neq z$ ;
- (Triangle inequality)  $\underbrace{d_{F1}(\{x\}, \{z\})}_1 > \underbrace{d_{F1}(\{x\}, \{y\})}_0 + \underbrace{d_{F1}(\{y\}, \{z\})}_0$ .

By altering the reference and prediction sets, it can be shown that the value of precision and recall are switched. However,  $F1$  is symmetrical between the precision and recall and therefore it has the symmetry property.

*Average Precision (AP)* is a similarity measure and it is normalized between 0 and 1. The true positives, false positives and false negatives are determined via matching the reference set to the predictions set greedily with higher confidence score prediction is matched first. Let denote the precision in the order of confidence score as  $p$  and recall as  $r$ , the AP score, which is the area under the  $p(r)$  curve, has the exact form of

$$AP = \int_0^1 p(r) dr. \quad (2)$$

In practice, this area is approximated by calculating the average value over a set of recall points (11 points in Pascal VOC [19] and 101 points in COCO challenge [39]). In particular, given  $r_1, \dots, r_N$  are  $N$  selected recall points for the



approximation such that  $r_n < r_{n+1}, \forall n < N$ , the approximated AP score is calculated as:

$$\widetilde{AP} = \sum_{n=1}^{N-1} (r_{n+1} - r_n) \widetilde{p}(r_{n+1}), \quad (3)$$

where  $\widetilde{p}(r)$  is the approximation of  $p(r)$  such that  $\widetilde{p}(r) = \max_{\tilde{r} \geq r} p(\tilde{r})$ .

For the example in Fig. 1, with one prediction and reference in each scenario, AP is turned into the calculation of the precision only<sup>1</sup>. Following the same argument given for F1,  $p = 1$  for the both pair scenarios  $(x, y)$  and  $(y, z)$ , but  $p = 0$  for the pair scenario  $(x, z)$ . Consequently,  $d_{AP}$  does not fulfill identity and triangle inequality as

- (Identity)  $d_{AP}(\{x\}, \{y\}) = d_{AP}(\{y\}, \{z\}) = 0$ , but  $x \neq y \neq z$ ;
- (Triangle inequality)  $\underbrace{d_{AP}(\{x\}, \{z\})}_1 > \underbrace{d_{AP}(\{x\}, \{y\})}_0 + \underbrace{d_{AP}(\{y\}, \{z\})}_0$ .

The approximated  $\widetilde{AP}$  dissimilarity measure also trivially violates the above metric properties in the same example. Moreover, AP as area under precision-recall curve in exact form of Eq. (2) is symmetrical, but this property cannot be guaranteed in the approximation, *i.e.*,

- $d_{\widetilde{AP}}(\{x\}, \{y\}) \neq d_{\widetilde{AP}}(\{y\}, \{x\}) \forall x, y \in \mathbb{X}$ , where  $\mathbb{X}$  is the space of all possible predictions.

Note that, as mAP is the average of AP over all classes, it is also not a (mathematical) metric.

*Log-Average Miss Rate (log-AMR)* is a dissimilarity measure which takes values between 0 and 1. The truth-to-prediction matches are determined in similar manner as for the calculation of AP score. For the miss rate  $m$  and false positives per image rate (FPPI)  $f$  (sorted in the order of the prediction score), the log-AMR is calculated as

$$AMR = \exp \left( \frac{1}{N} \sum_{n=1}^N \ln(m(f_n)) \right), \quad (4)$$

where  $f_1, \dots, f_N$  are sampled FPPI rates used in the calculation. In the original implementation [17],  $f_1, \dots, f_N$  are chosen as 9 samples evenly spaced in log space, specifically,  $f_1 = 10^{-2}, f_2 = 10^{-1.75}, \dots, f_9 = 10^0$ .

We define the dissimilarity measure form of log-AMR as itself, *i.e.*,  $d_{\text{log-AMR}} = AMR$ . From the formulation, this dissimilarity measure has the same property as the abstract dissimilarity measure defined in the 1-D counter

<sup>1</sup>there is a single prediction with an arbitrary score. Therefore, there exist no range for the confidence score.

example of the main text (for the pair of two singleton sets). In Fig. 1, for the pair scenarios  $(x, y)$  and  $(y, z)$ , both the miss rate and FPPI rate are zero hence  $d_{\text{Log-AMR}}(\{x\}, \{y\}) = d_{\text{Log-AMR}}(\{y\}, \{z\}) = 0$ . For the pair scenario  $(x, z)$ , the miss rate and FPPI rate are both 1 hence  $d_{\text{Log-AMR}}(\{x\}, \{z\}) = 1$ . Therefore, the triangle inequality and identity property do not hold.

- (Identity)  $d_{\text{Log-AMR}}(\{x\}, \{y\}) = d_{\text{Log-AMR}}(\{y\}, \{z\}) = 0$ , but  $x \neq y \neq z$ ;
- (Triangle inequality)  $\underbrace{d_{\text{Log-AMR}}(\{x\}, \{z\})}_1 > \underbrace{d_{\text{Log-AMR}}(\{x\}, \{y\})}_0 + \underbrace{d_{\text{Log-AMR}}(\{y\}, \{z\})}_0$ .

In addition, as the averaging step to calculate log-AMR is carried out over a finite samples of FPPI rate, the symmetrical property cannot be guaranteed, *i.e.*,

- $d_{\text{Log-AMR}}(\{x\}, \{y\}) \neq d_{\text{Log-AMR}}(\{y\}, \{x\}) \forall x, y \in \mathbb{X}$ , where  $\mathbb{X}$  is the space of all possible predictions.

Furthermore, AP and log-AMR rely on the greedy assignment to match the true to the predicted objects. This approach is indeed sub-optimal as the score and the geometrical similarity of the objects are treated independently, where the geometrical matches are conditioned on the order of the confidence score. To this extent, in Subsection 4.1, via our proposed IoU/GIoU extension to confidence score, we introduce a new approach to compute AP and log-AMR optimally which is shown to produce more meaningful predictions ranks in the experiment of Subsection D.4.

*MOTA* is a similarity measure taking any values between  $-\infty$  and 1. Specifically, given  $FP_t, FN_t, IDSW_t$  and  $GT_t$  are respectively the number of false positives, false negatives, ID switches and ground truth track instances at time  $t$ , the MOTA score is calculated as [5]:

$$MOTA = 1 - \frac{\sum_t FP_t + FN_t + IDSW_t}{\sum_t GT_t}. \quad (5)$$

Following the same argument as above, the bounding box (as a single frame track)  $x$  can be considered as a true positive for the track  $y$  ( $FP_t = FN_t = IDSW_t = 0$  and  $d_{MOTA}(\{x\}, \{y\}) = 0$ ), and the track  $y$  can be considered as a true positive for the track  $z$  ( $FP_t = FN_t = IDSW_t = 0$  and  $d_{MOTA}(\{y\}, \{z\}) = 0$ ). However, the track  $x$  is considered as false positive for the track  $z$ ; therefore, there is one false positive and false negative ( $FP_t = FN_t = 1$  and  $d_{MOTA}(\{y\}, \{z\}) = 2$ ). Consequently, *MOTA* does not fulfill metric properties, *i.e.*,

- (Identity)  $d_{MOTA}(\{x\}, \{y\}) = d_{MOTA}(\{y\}, \{z\}) = 0$ , but  $x \neq y \neq z$ ;

- (Triangle inequality)  $\underbrace{d_{MOTA}(\{x\}, \{z\})}_2 > \underbrace{d_{MOTA}(\{x\}, \{y\})}_0 + \underbrace{d_{MOTA}(\{y\}, \{z\})}_0.$

Due to its sequential process to indicate ID switches over time, it can be also shown that *MOTA* does not fulfill the symmetry property, *i.e.*,

- $d_{MOTA}(\{x\}, \{y\}) \neq d_{MOTA}(\{y\}, \{x\}) \forall x, y \in \mathbb{T}$  where  $\mathbb{T}$  is the space of all possible predicted tracks.

*IDF1* is the similarity measure which can take value between 0 and 1 and it is defined as [44]:

$$IDF1 = \frac{2IDTP}{2IDTP + IDFP + IDFN}, \quad (6)$$

where *IDTP*, *IDFP* and *IDFN* are respectively the numbers of true positive ID, false positive ID and false negative ID. Similar to the *MOTA* example, *IDF1* dissimilarity measure between pairs of single-frame tracks  $(x, y)$  and  $(y, z)$  are  $d_{IDF1}(\{x\}, \{y\}) = d_{IDF1}(\{y\}, \{z\}) = 0$  as the numbers of false negative ID and false positive ID are 0 and the number of true positive ID is 1. For the pair of single-frame track  $(x, z)$  the *IDF1* dissimilarity measure is  $d_{IDF1}(\{x\}, \{z\}) = 1$  as the number of true positive ID is 1 and there are no false positive ID and false negative ID. Hence the *IDF1* in dissimilarity measure form violates the following metric properties:

- (Identity).  $d_{IDF1}(\{x\}, \{y\}) = d_{IDF1}(\{y\}, \{z\}) = 0$ , but  $x \neq y \neq z$ ;
- (Triangle inequality)  $\underbrace{d_{IDF1}(\{x\}, \{z\})}_1 > \underbrace{d_{IDF1}(\{x\}, \{y\})}_0 + \underbrace{d_{IDF1}(\{y\}, \{z\})}_0.$

In the extended experimental Subsection D.1, we further illustrate how mathematical inconsistency affects the behaviours of the performance criteria.

## B. Further Discussions on Guidelines for Selection of Performance Criteria

In the main text, we have advocated the necessity of mathematical consistency, meaningfulness and ranking reliability of a performance criterion. Moreover, the importance of mathematical consistency has been discussed in the previous section. In this section, we further clarify the rationale behind our sanity test (Section 3(ii) of the main text) and provide extended discussions on its features. In addition, we also provide details on three intuitive indicators that can be used to measure the reliability of a performance criterion with respect to variation of hyper-parameters.

### B.1. Meaningfulness and sanity test

Our proposed sanity-testing strategy considers the perturbations of truth sets, independent of the scene context, to form prediction sets. In particular, for a given set of perturbation types, we generate a set of predictions from the parameters characterizing the perturbation (*e.g.* number of misses, falses, amount of dislocation, confidence score, *etc.*), such that given this information one can easily distinguish the ranking order of the predictions, independently from the procedure how the predictions are generated.

It is not necessary that the performance of the predictions are clearly distinguishable via visual inspection (without any prior information or context). Let consider examples in Fig. 2, via visual inspection, it is almost impossible for anyone to distinguish the performance of prediction (a) and prediction (b) but via the parameters characterizing the perturbations (the dislocation amount) one can easily tell that prediction (a) is better than prediction (b) (lower dislocation amount). Similarly, without the context, it is very uncertain to differentiate the performance between prediction (c) and prediction (d) due to the complexity of the scene, however, given the amount of dislocation, number of misses, falses, one can easily tell (c) is better than (d).

**Remark:** We note that the ambiguity of the test is undeniable as the context is not taken into account during the construction of the test. Hence, we do not expect any existing performance criteria that do not incorporate the contextual information into the evaluation scheme to achieve zero ranking error although the ranking order is clear (from the abstract perspective). It is also worth noting that in many real scenarios, even if the parameters characterizing the perturbations are given, one may not be able to differentiate the performance between predictions, *i.e.*, predictions (e) and (f) in Fig. 2. In those cases, we shall solely rely on the criteria to rank those predictions.

### B.2. Assessing the performance criteria reliability

The reliability of a performance criterion is indicated by its variation over the range of hyper-parameter values. In this context, we refer to this property as *ranking consistency*. While there are many ways that we can measure this consistency, we are particularly interested in the *purity* of the ranking order, its *distortion level* and its *sensitivity* to the change of hyper-parameter.

Specifically, to measure the purity of the ranks across  $m$  independent hyper-parameters, we calculate the average number of ranking switches per predictions set. For an  $m$ -D vector  $\varrho^{(i)}$  of the ranks of prediction set  $i^{th}$  across  $m$  hyper-parameters, the number of ranking switches is given by  $R_S^{(i)} = |\{\varrho^{(i)}[j] : j \in \{1, \dots, m\}\}| - 1$ . The *average ranking switches per set* is given by  $\overline{R_S} = \sum_{i=1}^K R_S^{(i)} / K$ , where  $K$  is the number of predictions sets in consideration.

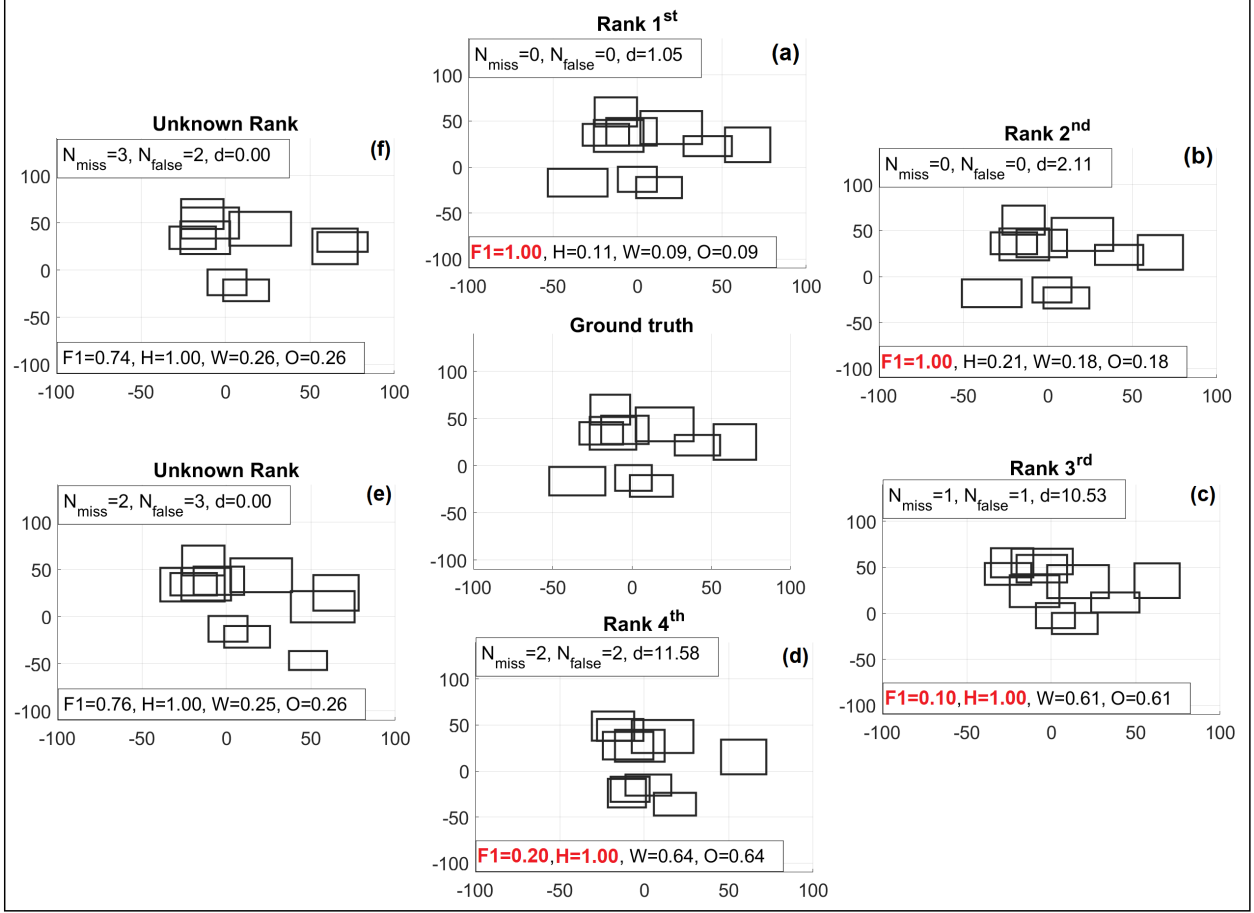


Figure 2: Visual demonstration on the concept of parameters characterizing the perturbation in the sanity test where  $N_{\text{miss}}$ ,  $N_{\text{false}}$  are the number of missed and false objects,  $d$  is the dislocation of centroid (Euclidean distance); **F1** is the F1 score at IoU=0.5 (higher better); **H**, **W** and **O** are respectively Hausdorff, Wasserstein and OSPA metrics with IoU base distance (lower better). Prediction (a) is very competitive compared to prediction (b). It is uncertain to tell if (c) is better than (d) by visual inspection but it is clear via parameters characterizing the perturbation. Interestingly, Wasserstein and OSPA metrics can distinguish the performance of scenarios correctly while Hausdorff metric cannot rank the pair (c)-(d) and F1 score produces wrong ranking order. It is uncertain to rank (e) and (f) via either visualisation or parameters characterizing the perturbation hence we need to solely rely on evaluation criteria to rank them in this case.

On the other hand, the degree of distortion of the ranks is reflected in the standard deviation of the elements of  $\rho^{(i)}$ . For the  $i^{\text{th}}$  set, the ranking distortion is defined as  $R_{\text{std}}^{(i)} = \text{std}(\rho^{(i)})$  and average ranking distortion per set as  $\overline{R_{\text{std}}} = \sum_{i=1}^K R_{\text{std}}^{(i)} / K$ , where  $\text{std}(\cdot)$  is the function to calculate the standard deviation of elements of the vector in its argument.

To indicate the ranking consistency given the sequential nature of the thresholds, we can measure the sensitivity of the ranking order against the change of hyper-parameters via taking its first order derivative with respect to the thresholds. In particular, let  $\zeta_{t_1}^{(1)}, \dots, \zeta_{t_m}^{(K)}$  be the ranking vectors (tuple of the ranks) of methods 1 to  $K$  across  $m$  thresholds from  $t_1$  (sequentially) to  $t_m$ , the average ranking sensitivity across the set of these  $m$  thresholds is defined as  $\overline{R_{\text{sen}}} =$

$$\sum_{i=1}^K \sum_{j=1}^{m-1} \left| \left( \zeta_{t_j}^{(i)} - \zeta_{t_{j+1}}^{(i)} \right) / ((t_{j+1} - t_j) \times (m-1) \times K) \right|.$$

If the thresholds are evenly spaced the factor  $(t_{j+1} - t_j)$  can be omitted.

### C. Further Discussions on Metrics

In the main text, we propose an extension of IoU/GIoU to accommodate the confidence score implicitly in the calculation (Subsection 4.1) and the use of (mathematical) metrics as alternatives for the traditional performance criteria (Subsection 4.2). In this section, we present detailed implementation of the proposed IoU/GIoU extension and further discussions on the existing point pattern metrics in the literature.

### C.1. Metric for shapes and confidence score

Traditional IoU and GIoU measures only reflect the similarity between shapes geometrically but not the confidence scores of the predictions. In the main text, we propose a new method to calculate IoU/GIoU by extending the shapes to an extra dimension to accommodate the confidence score (via taking Cartesian product between the shape and corresponding score). In this subsection, we provide the readers with the details to implement the proposed extension via the pseudo-code given in Alg. 1. Note that as  $V_x$  and  $V_y$  in Alg. 1 are convex shapes, this extension of IoU/GIoU to the confidence score inherits all mathematical properties discussed in [43].

---

#### Algorithm 1: IoU/GIoU extension to confidence score

---

**input:** two arbitrary  $N$ -D convex shapes,  $x, y$  and their corresponding confidence score,  $0 < s_x \leq 1$  and  $0 < s_y \leq 1$ .

**output:** Standard IoU/GIoU distance,  $d_{IoU}(x, y)$ ,  $d_{GIoU}(x, y)$ ; extended IoU/GIoU distance,  $d_{\widetilde{IoU}}(x, s_x, y, s_y)$ ,  $d_{\widetilde{GIoU}}(x, s_x, y, s_y)$

For  $x$  and  $y$ , find the smallest enclosing convex object  $C$ , then

$$\begin{aligned} IoU &= \frac{|x \cap y|}{|x \cup y|}, \\ d_{IoU} &= 1 - IoU, \\ GIoU &= IoU - \frac{|C \setminus (x \cup y)|}{|C|}, \\ d_{GIoU} &= \frac{1 - GIoU}{2}. \end{aligned}$$

Construct  $V_x$  and  $V_y$ , the  $N+1$ -D shapes which are Cartesian products of  $x$  and  $y$  with  $s_x$  and  $s_y$  respectively.

For  $V_x$  and  $V_y$ , find the smallest enclosing convex object  $V_C$ , then

$$\begin{aligned} \widetilde{IoU} &= \frac{|V_x \cap V_y|}{|V_x \cup V_y|}, \\ d_{\widetilde{IoU}} &= 1 - \widetilde{IoU}, \\ \widetilde{GIoU} &= \widetilde{IoU} - \frac{|V_C \setminus (V_x \cup V_y)|}{|V_C|}, \\ d_{\widetilde{GIoU}} &= \frac{1 - \widetilde{GIoU}}{2}. \end{aligned}$$


---

As discussed previously, current implementation of AP and log-AMR rely on the greedy assignment to determine the truth-to-prediction matches which does not guarantee the optimality of the matches. Basing on this extension, we propose an alternative strategy to compute AP (mAP) and log-AMR (can be extended to other criteria relying on greedy assignment). Particularly, we first calculate the pair-wise similarity scores between true and predicted objects via the IoU/GIoU extension. We then propose the use of optimal assignment algorithm to determine the matches. Given the optimal matches and a threshold value, we can determine the numbers of true positives, false positives, false negatives and then sort them in the order from the highest to the lowest

confidence score. Subsequently, the standard computation for AP or log-AMR is carried out. As this approach takes into account both the confidence score and the geometrical similarity together, the assignment is indeed optimal. In Subsection D.5, we show that it produces more meaningful ranking order compared to the greedy assignment approach.

### C.2. Point pattern metrics

For completeness, this section provides a brief review of the point pattern metrics (in Subsection 4.2 of the main text), and some additional remarks.

Consider a metric space  $(\mathbb{W}, \underline{d})$ , where  $\underline{d} : \mathbb{W} \times \mathbb{W} \rightarrow [0; \infty)$  is the *base-distance* between the elements of  $\mathbb{W}$ . The Hausdorff distance between two non-empty point patterns  $X$  and  $Y$  of  $\mathbb{W}$  is defined by [21, 26]

$$d_H(X, Y) = \max \left\{ \max_{x \in X} \min_{y \in Y} \underline{d}(x, y), \max_{y \in Y} \min_{x \in X} \underline{d}(x, y) \right\}. \quad (7)$$

This metric was traditionally used as a measure of dissimilarity between binary images. It gives a good indication of the dissimilarity in the visual impressions that a human would typically perceive between two binary images.

In general, the Wasserstein distance (also known as Mallows distance) of order  $p \geq 1$  between two non-empty point patterns  $X = \{x_1, \dots, x_m\}$  and  $Y = \{y_1, \dots, y_n\}$  is defined by [16, 26]

$$d_W^{(p)}(X, Y) = \min_C \left( \sum_{i=1}^m \sum_{j=1}^n c_{i,j} \underline{d}(x_i, y_j)^p \right)^{\frac{1}{p}}, \quad (8)$$

where  $C = (c_{i,j})$  is an  $m \times n$  transportation matrix, *i.e.*, the entries  $c_{i,j}$  are non-negative, each row sum to  $1/m$ , and each column sum to  $1/n$ . The order  $p$  in the Wasserstein distance plays the same role as the order of the  $\ell_p$ -distance for vectors, which is usually assumed to be 1 or 2 in most applications.

For an IoU/GIoU base-distance, which is a ratio of hypervolumes, the Wasserstein distance of order 1 has a more natural interpretation than its higher order counterparts. This special case is commonly known as the Earth mover's distance. If we consider the sets  $X$  and  $Y$  as collections of earth piles and suppose that the cost of moving a mass of earth over a distance is given by the mass times the distance. Then the Earth mover's distance can be considered as the minimum cost needed to build one collection of earth piles from the other.

Note that, in general, the Hausdorff and Wasserstein metrics are not defined when either of the set is empty. This is problematic for performance evaluation because it is not uncommon for the prediction set or reference set to be empty. However, when  $\underline{d}$  is bounded by 1 (as per the IoU/GIoU distance), this problem can be resolved (while observing the



metric properties) by defining  $d_H(X, Y) = d_W^{(p)}(X, Y) = 1$  if one of the set is empty, and  $d_H(\emptyset, \emptyset) = d_W^{(p)}(\emptyset, \emptyset) = 0$ .

In its general form, the Optimal Sub-Pattern Assignment (OSPA) distance of order  $p \geq 1$ , and cut-off  $c > 0$ , between two point patterns  $X = \{x_1, \dots, x_m\}$  and  $Y = \{y_1, \dots, y_n\}$  is defined by [49]

$$d_0^{(p,c)}(X, Y) = \left( \frac{1}{n} \left( \min_{\pi \in \Pi_n} \sum_{i=1}^m \underline{d}^{(c)}(x_i, y_{\pi(i)})^p + c^p (n - m) \right) \right)^{\frac{1}{p}}, \quad (9)$$

if  $n \geq m > 0$ , and  $d_0^{(p,c)}(X, Y) = d_0^{(p,c)}(Y, X)$  if  $m > n > 0$ , where  $\Pi_n$  is the set of permutations of  $\{1, 2, \dots, n\}$ ,  $\underline{d}^{(c)}(x, y) = \min(c, \underline{d}(x, y))$ . Further  $d_0^{(p,c)}(X, Y) = c$  if one of the set is empty, and  $d_0^{(p,c)}(\emptyset, \emptyset) = 0$ . The order  $p$  plays the same role as per the Wasserstein distance, and is taken to be 1 in this work. The cut-off parameter  $c$  provides a weighting between cardinality and location errors. A large  $c$  emphasizes cardinality error while a small  $c$  emphasizes location error. However, a small  $c$  also decreases the sensitivity to the separation between the points due to the saturation of  $\underline{d}^{(c)}$  at  $c$ . The reader is referred to [49] for a discussion/comparison of the Hausdorff, Wasserstein and OSPA metrics.

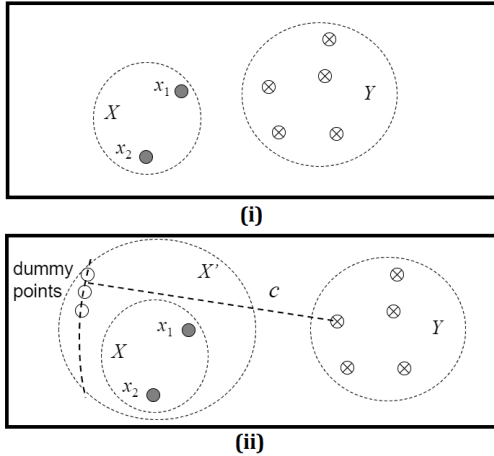


Figure 3: OSPA distance between  $X$  and  $Y$  as the average distance between the best pairing of the points of  $X'$  and  $Y$ .

The general OSPA distance above yields the following base-distance between two tracks  $f$  and  $g$ :

$$\underline{d}^{(c)}(f, g) = \sum_{t \in \mathcal{D}_f \cup \mathcal{D}_g} \frac{d_0^{(c)}(\{f(t)\}, \{g(t)\})}{|\mathcal{D}_f \cup \mathcal{D}_g|},$$

if  $\mathcal{D}_f \cup \mathcal{D}_g \neq \emptyset$ , and  $\underline{d}^{(c)}(f, g) = 0$  if  $\mathcal{D}_f \cup \mathcal{D}_g = \emptyset$ , where  $d_0^{(c)}$  denotes the OSPA distance (the order parameter  $p$  is

redundant because only sets of at most one element are considered) [2]. Note that, apart from the tracking error over the entire scenario, the OSPA<sup>(2)</sup> distance (OSPA distance with the above base-distance) between two sets of tracks can be plotted against time. Two algorithms can with similar OSPA<sup>(2)</sup> errors over the entire scenario, may exhibit different OSPA<sup>(2)</sup> error curves over time. The monitoring of the tracking performance over time is important for the analysis/diagnosis of tracking algorithms. We refer the interested reader to [2] for more details.

The OSPA distance treats a cardinality error as if the set with smaller cardinality contained an additional (dummy) point separated from the remaining set by a base-distance of at least  $c$ . For an IoU/GIoU base-distance, such dummy point does not exist when the cut-off  $c > 1$ , because the largest possible separation between any two points in  $\mathbb{W}$  is 1. Hence, there is no physical meaning in penalizing a cardinality error with an IoU/GIoU base-distance of  $c > 1$ . On the other hand, to ensure sensitivity to all IoU/GIoU base-distance separations, we require  $c \geq 1$ . Consequently, for an IoU/GIoU base-distance, the best cut-off choice for the OSPA distance is  $c = 1$ , as per Eqs. 1 of Section 4 of the main text.

As alluded to in Sections 3 and 4 of the main text, it is obvious that a criterion should not assign a larger error to a scenario with an accurate prediction than a (different) scenario with an inaccurate prediction. Hence, it is necessary to sanity-test a criterion across different scenarios, along the line of the example in Fig. 2. Due to the page restriction, such sanity tests were not presented in Section 5. The tests presented in Section 5 only compare a criterion's ranking of predicted sets (against their pre-determined ranking) within each scenario.

For completeness, we now present a sanity test that assesses the criterion's meaningfulness across different scenarios numbered from 1 to 10. In scenario  $k$ , the number of true objects is  $2^k$ . The objects are 1cm by 1cm squares, evenly spaced so that the nearest object is more than 2cm away. The prediction set is the true set with each object shifted to the left by  $2^{-0.5k}$  cm. Since the predicted cardinality is correct, unequivocally, scenario 1 must have larger prediction error than scenario 2 and so on as the localization error decreases from scenario 1 to scenario 10. .

Fig. 4 plots the  $F1_{IoU}$  prediction error ( $1 - F1_{IoU}$ ),  $OSPA_{IoU}$ , un-normalized  $OSPA_{IoU}$ ,  $Wasserstein_{IoU}$ , and  $Hausdorff_{IoU}$  distances for each scenario. Note that the  $Wasserstein_{IoU}$ ,  $Hausdorff_{IoU}$  and  $OSPA_{IoU}$  distances exhibit identical behaviour that corroborate with physical intuition as they decrease with better performance. The  $F1_{IoU}$  distance can only take the value of either 0 or 1, and is not granular enough to distinguish the prediction errors in scenarios 1, 2 and 3 to 10. Nonetheless, it still shows the general trend of improving performance. In contrast, the un-normalized

OSPA<sub>IoU</sub> metric produces non-sensical prediction error that increases drastically with unequivocally better performance.

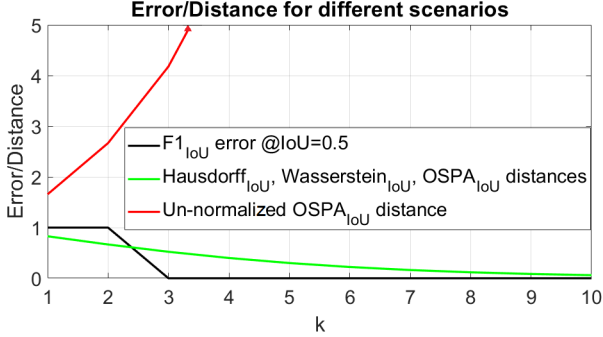


Figure 4: The distances between true and predictions sets in scenario  $k$  of the sanity test with only dislocation of the centroid.

## D. Extended Experimental Results

In Subsection D.1, we first provide experiments to further illustrate the significance of mathematical inconsistency on the performance criteria mentioned in Section 2. Subsection D.2 supplements Subsection 5.1 of the main text with further descriptions on the sanity tests and more detailed results. More illustrations on the influence of mathematical consistency over the evaluation performance is given in Subsection D.3. In Subsection D.4, we present some insights on the evaluation results of real dataset experiments in Subsection 5.2 of the main text. Finally, in Subsection D.5, we demonstrate that our proposed optimal assignment approach for mAP and log-AMR criteria in Subsection C.1 indeed improve their performance in terms of the accuracy (meaningfulness) of the ranks.

### D.1. Significance of mathematical inconsistency

Since mathematical consistency/inconsistency can be established analytically, and requires no sanity-testing, an illustration of its importance to trustworthiness has not been presented. This subsection presents experiments to illustrate the tangible effect of mathematical consistency on the trustworthiness of performance criteria.

For the detection experiment, we first generate a set of random bounding boxes as the ground-truth set as per Section 5 of the main text. We then generate the approximate-truth set by perturbing the ground-truth set with small dislocations (at least 0.9 IoU threshold between true and approximate true boxes). Predictions are generated by perturbing the ground-truth set with larger dislocations (compared to the approximate-truth, *i.e.* IoU thresholds between true and predicted boxes of approximately 0.55). The experiments are performed over 100 Monte Carlo trials

<sup>1</sup>This distance takes same the form as Eqs. 9 but without the normalizing constant  $1/n$ .

Similarly, for the tracking experiment, we generate ground-truth set of tracks across temporal domain of 100 time steps (via a constant velocity model) as per Section 5 of the main text. The approximate-truth and predicted sets of tracks are generated, respectively, by perturbing the centroids of ground-truth tracks at each time step with small dislocations (at least 0.9 IoU threshold between true and approximate true boxes), and larger dislocations (IoU thresholds between true and predicted boxes of approximately 0.55).

We examine the  $F1_{IoU}$  and  $mAP_{IoU}$  dissimilarity measures, *i.e.*  $1 - F1_{IoU}$  and  $1 - mAP_{IoU}$ , and the OSPA<sub>IoU</sub> distance. Note that the mAP score is calculated by assuming there is only 1 class and the confidence score is 0.9 for all predictions. In terms of mathematical consistency, the Hausdorff and Wasserstein distances behave similarly to OSPA, and are omitted. The dissimilarity between approximate-truth and ground-truth, true prediction error, and approximate prediction error, are plotted against the number of Monte Carlo trials in Fig. 5. The approximate OSPA (and Hausdorff and Wasserstein) prediction error closely resemble the true prediction error. In contrast, using traditional criteria, the approximate prediction error fluctuate among trials, while the true prediction error saturates at maximum separation for most of the trials.

### D.2. Details on sanity tests

This subsection provides additional details and results on the sanity tests presented in the main text, along with an experiment on single-class multi-object detection to compare the metrics with the traditional F1 score.

#### D.2.1 Multi-class multi-object detection test

##### Experiment settings

To construct the test, we first uniformly sample a set of  $N_D$  bounding boxes (capped at maximum 40 boxes) as our reference set. The centroids range is  $[-200, 200] \times [-200, 200]$  and the sizes range is  $[20, 40]$ . Each true box is assigned a random enumerated class between 1 and 5. The confidence scores for the true boxes are one. We then generate 20 sets of predictions (produced by 20 hypothetical detectors) by introducing disturbances to the sampled reference set. In addition to the bounding boxes state, each prediction has a confidence score taking value between 0 and 1. In this experiment, we consider the perturbation on the dislocation of the centroid (in terms of Euclidean distance), small disturbance on the size, the number of mis-detections, state-dependent falses, random falses and mis-classifications.

To simulate noise on dislocation and confidence score, we sequentially assign each reference box with a distinct label. For each predictions set, we construct a function to control the amount of the centroid dislocation and the

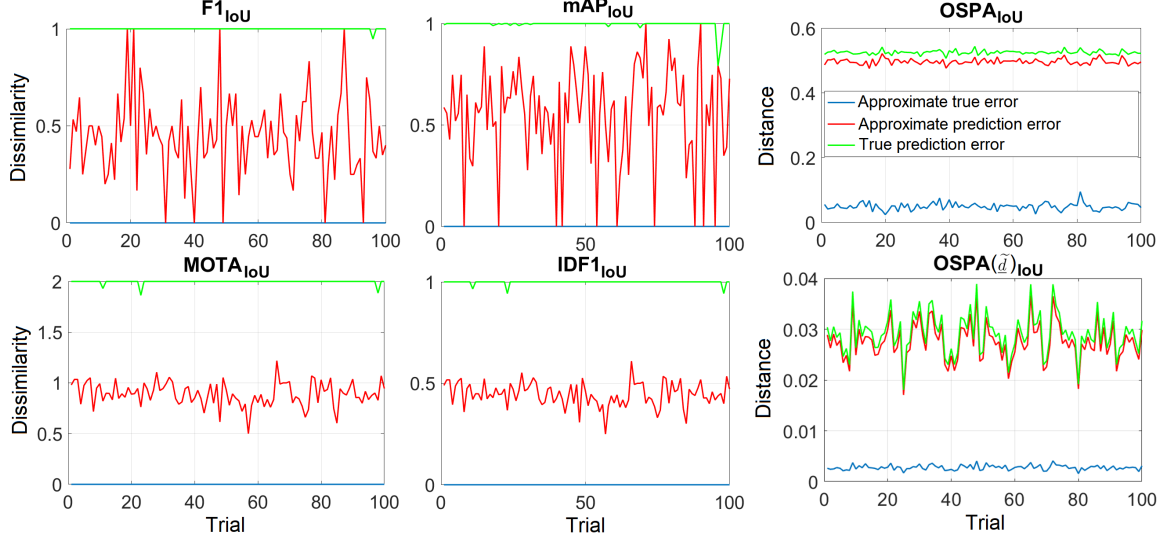


Figure 5: Dissimilarities/Distances between true, approximate true and prediction sets for traditional criteria and OSPA metrics in the detection experiment (top row) and tracking experiment (bottom row). The inconsistent relationships between them is observed in traditional criteria but not in OSPA metrics.

reduction (from 1) of the prediction confidence score. In this experiment, we utilise the function  $d^{(k)}(n) = a^{(k)} \times n$  to control the amount of centroid dislocation, where  $d^{(k)}(n)$  is the centroid dislocation of the object with distinct label  $n$  in the predictions set  $k^{th}$ ,  $a^{(k)}$  is a unique constant for the predictions set  $k^{th}$ . Similarly, the reduction of confidence score is controlled by the function  $r^{(k)}(n) = b^{(k)} \times n$ , where  $r^{(k)}(n)$  is the confidence score reduction of the object with distinct label  $n$  in the predictions set  $k^{th}$ ,  $b^{(k)}$  is a constant associating with the predictions set  $k^{th}$ .

For 20 sets of predictions, the constant  $a^{(k)}$  for the  $k^{th}$  set is calculated as following. We first generate  $D$ , a 20-D vector whose elements are evenly spaced (in ascending order) numbers from 10 to 20. The constant  $a^{(k)}$  is then calculated as  $a^{(k)} = D[k]/N_D$ . Similarly, the constant  $b^{(k)}$  for the confidence score reduction control function is also calculated as  $b^{(k)} = S[k]/N_D$  where  $S$  is another 20-D vectors whose elements are evenly spaced (in ascending order) numbers from 0.2 to 0.8. For an object with label  $n$  and predicted by detector  $k$ , the dislocation in x-coordinate of the centroid is  $\Delta_x^{(n,k)} = u \times d^{(k)}(n)$  where  $u$  is a random number sampled between 0 and 1. The dislocation in y coordinate of the centroid is then calculated as

$$\Delta_y^{(n,k)} = \sqrt{(d^{(k)}(n))^2 - (\Delta_x^{(n,k)})^2}. \quad (10)$$

Let  $u_2$  be a 2-D vector whose elements are random number drawing between 0 and 1, if  $u_2[1] < 0.5$  then  $\Delta_x^{(n,k)} = -\Delta_x^{(n,k)}$  and if  $u_2[2] < 0.5$  then  $\Delta_y^{(n,k)} = -\Delta_y^{(n,k)}$ . The confidence score of this prediction is simply  $\varsigma_n^{(k)} = 1 - r^{(k)}(n)$ . In this test, each box has a small random disturbance on their size.

While the noise on dislocation and confidence score are introduced from the first predictions set, the cardinality mismatches are only introduced from the 11<sup>th</sup> predictions set. For each experiment, we sample the following 10-D vectors,  $P_D, P_C$  uniformly within the range  $[0.5, 0.95]$ ,  $F_S$  uniformly within the range  $[0.05, 0.5]$  and  $F_R$  as Poisson random numbers with the rates of  $[1 : 1 : 10]$  (1 to 10 in the step of 1). The elements of  $P_D, P_C$  are sorted in descending order and elements of  $F_S, F_R$  are sorted in the ascending order.

For a detector  $k$ , to simulate state-dependent false, we first calculate the number of the false as  $N_{F_R}^{(k)} = \text{round}(N_D \times F_S[k])$  (where  $\text{round}(\cdot)$  is the function to round the number in its argument to the nearest non-negative whole number). If an object is chosen to have state-dependent false, it has an extra object that has the same dislocation amount and the same confidence score as the corresponding predicted object. The number of mis-detections is given as  $N_M^{(k)} = \max((N_D - N_{F_R}^{(k)}) \times (1 - P_D[k]), 0)$ . Among the remaining objects (not having state-dependent false), the objects that are chosen to be missed are the objects that have the highest values of the distinct labels, i.e., objects that have highest distortion in terms of dislocation and lowest confidence score. Subsequently, the number of mis-classified objects is given as  $N_C^{(k)} = \max((N_D - N_{F_R}^{(k)} - N_M^{(k)}) \times (1 - P_C[k]), 0)$ . The mis-classified objects are chosen such that the ones with highest enumerated labels are selected. Finally, the number of random false positives is  $F_R$ . The false positive boxes are sampled following the same procedure as of sampling the reference boxes.

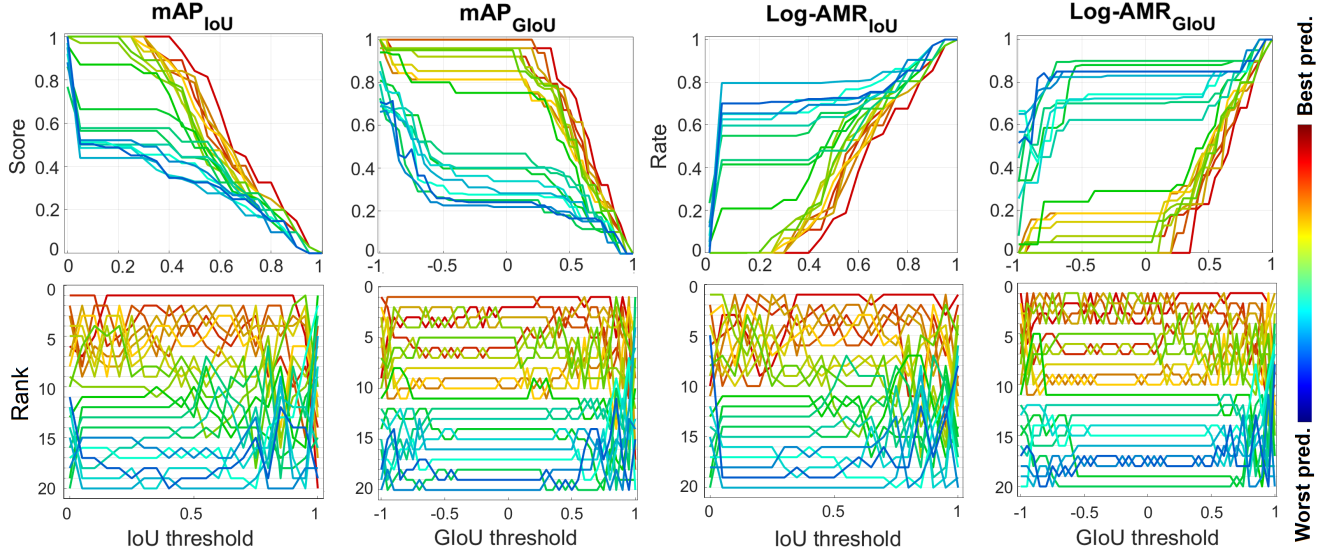


Figure 6: mAP score and log-AMR (top row) and the corresponding ranks of predictions (bottom row) over a range of IoU/GIoU thresholds in one trial of the multi-class multi-object detection sanity test. The pre-determined ranks are color-coded from worst (blue) to best (red).

Table 1: Means (and standard deviations) of the ranking consistency indicators for traditional criteria in multi-class multi-object detection sanity test over all experiment trials.

Multi-class multi-object detection				
	mAP <sub>IoU</sub>	Log-AMR <sub>IoU</sub>	mAP <sub>GIoU</sub>	Log-AMR <sub>GIoU</sub>
$\overline{R_S}$	7.9 (1.8)	<b>7.7 (1.8)</b>	8.4 (2.0)	8.4 (2.0)
$\overline{R_{std}}$	3.5 (0.9)	3.2 (0.8)	2.7 (0.7)	<b>2.5 (0.7)</b>
$\overline{R_{Sen}}$	3.6 (0.8)	3.6 (0.7)	3.5 (0.8)	<b>3.5 (0.7)</b>

### Extended results on the test

Both the scores and corresponding ranks of mAP and log-AMR with IoU and GIoU base measures are given in Fig. 6. While the ranking plots show the unreliability of the traditional criteria, the score plots demonstrate the behaviours of the criteria across the range of thresholds in a particular trial of the test. These plots show that the mAP score decreases and log-AMR increases in the direction from low to high thresholds. They also show that the differences between the scores at low and high extremes are narrow which leads to higher unreliability at the two ends of the thresholds range. The ranking reliability of the traditional criteria over all trials of the test is shown in Tab. 1 which indicates that the log-AMR is slightly better than mAP in terms of ranking reliability in our sanity test. Specifically, the log-AMR with GIoU base measure is better than its IoU counterpart in terms of lower ranking distortion and sensitivity to the change of hyper-parameter.

### D.2.2 Single-class multi-object detection test

In this experiment, we conduct the sanity test with single-class multi-object detection. The procedures to sample the reference and predictions sets are similar to the multi-class multi-object detection test except the simulation for confidence scores and the classes are not included.

Table 2: Means (and standard deviations) of the ranking consistency indicators for F1 score in sanity tests over all Monte Carlo trials.

Single-class multi-object detection		
	F1 <sub>IoU</sub>	F1 <sub>GIoU</sub>
$\overline{R_S}$	<b>7.9 (1.1)</b>	9.2 (1.4)
$\overline{R_{std}}$	3.5 (0.7)	<b>3.0 (0.6)</b>
$\overline{R_{Sen}}$	3.5 (0.7)	<b>3.1 (0.6)</b>

We present the F1 score across different IoU/GIoU thresholds and the corresponding ranking order for a particular trial of the test in Fig. 7. The result shows that the ranks vary significantly across range of IoU/GIoU thresholds and the



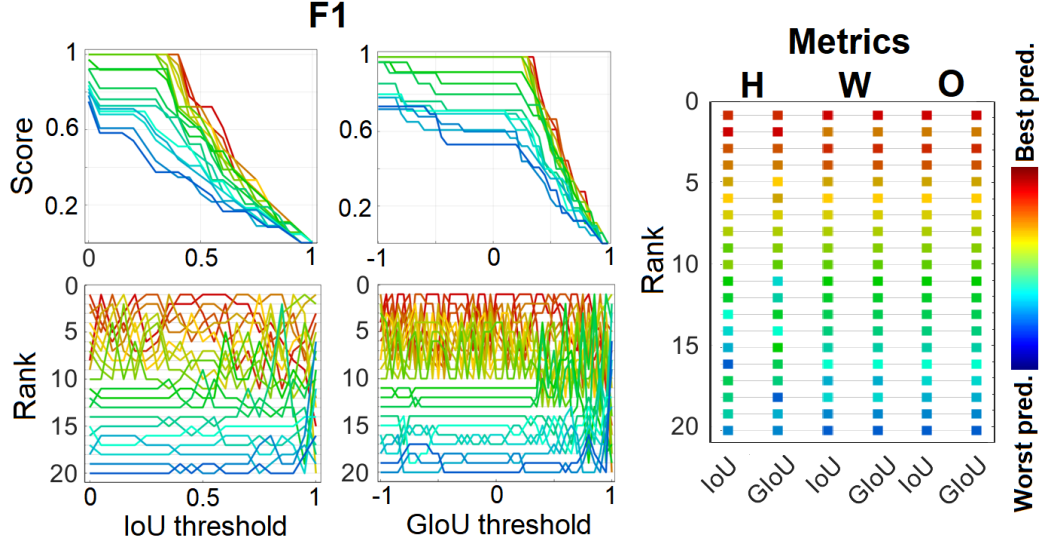


Figure 7: Left: F1 score (top row) and the corresponding ranks of predictions (bottom row) over a range of IoU/GIoU thresholds; right: ranks of predictions via Hausdorff (H), Wasserstein (W) and OSPA (O) metrics in one trial of the single-class multi-object detection sanity test. The pre-determined ranks are color-coded from worst (blue) to best (red).

F1 score exhibits similar behaviour as the mAP score in the sanity test with multi-class. The ranks via metrics show Wasserstein and OSPA metrics produce correct ranks of predictions sets for both IoU and GIoU base distances but the ranks are inconsistent and less meaningful in the case of Hausdorff metric. The ranking consistency over all trials of the test for F1 score is demonstrated in Tab. 2 which shows the F1 with GIoU base measure performs better than the IoU counterpart in terms of lower ranking distortion level and sensitivity to the change in hyper-parameter.

The ranking accuracy (meaningfulness) of various criteria over all trials is shown via Manhattan distance plots in Fig. 8. These results indicate that the F1 score at its optimal threshold performs better than the Hausdorff metric but worse than the Wasserstein and OSPA metrics with the latter performs better thanks to the balance penalization between the dislocation and cardinality errors. This observation is also further confirmed in Tab. 3. Furthermore, the accuracy of the marginalization approach over range of thresholds is indeed worse than the accuracy at the optimal threshold in the case of F1 score due to the strong dependency of the score on the thresholds (similar to mAP and log-AMR criteria with the thresholds marginalization approach).

### D.2.3 Multi-object tracking test

#### Experiment settings

In the tracking sanity test, we set the tracking window to 100 time steps and the number of tracks  $N_T$  in the reference set is randomly sampled between 5 and 30. The states of the tracks are sampled from the space of the bounding boxes

and each track is assigned a distinct enumerated label, *i.e.*, 1 to  $N_T$ . The length of the reference tracks are sampled between 50 and 100 time steps. The initial time of the track is then sampled between 1 and the latest possible initial time step given its length. The initial centroid of the tracks are sampled within the range  $[-200, 200] \times [-200, 200]$ .

For the initial size, we set a linear correlation between the height and the sampled initial y-coordinate of the tracks such that the height is limited within the range  $[20, 40]$  and the higher the y-coordinate the lower the height. After the height is calculated, the width is then calculated by multiplying the height with a random number being drawn within the range  $[0.5, 1.5]$ .

We then sample the course angles of the tracks uniformly from the range  $[0, 360]$  and their speeds uniformly within the range  $[1, 5]$ . From that, the velocity of the tracks are calculated. After the initialization, the centroids of the tracks follow the constant velocity model. To simulate the effect of in-out camera in the real tracking scenarios, the heights of the tracks vary linearly with their y-coordinate velocity and the minimum height is capped at 20. The width is kept unchanged through time.

In this test, we generate 20 sets of predictions (from 20 hypothetical trackers). The error types we consider here are the dislocation of centroids, sizes disturbances, missed tracks, tracks identities confusion (swapping) and false tracks (state-dependent and random). Following the same approach as in the multi-object detection test, at each time step, the amount of the centroid dislocation (in terms of Euclidean distance) is calculated basing on the enumerated labels of the tracks and the trackers performance. The amount of centroid dislocation



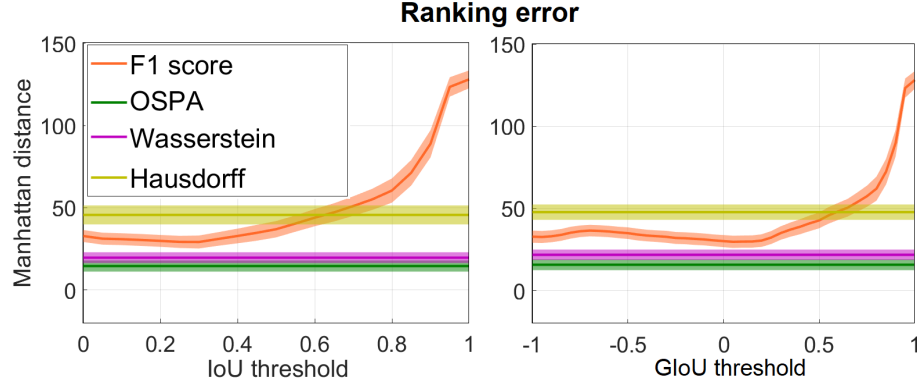


Figure 8: Mean Manhattan ranking errors (from the true ranking) of various criteria at different thresholds, over all Monte Carlo trials in single-class multi-object detection test. Shaded area around each curve indicates 0.2-sigma bound.

Table 3: Means (and standard deviations) of Manhattan ranking errors of various criteria at certain thresholds, over all Monte Carlo trials in the single-class multi-object detection sanity test. The subscripts of IoU/GIoU indicate the threshold values; "optimal" threshold is the one with best ranking accuracy; "M" threshold indicates that the evaluation is done via averaging the score over the range 0.5 to 0.95 in steps of 0.05.

Single-class multi-object detection test						
	IoU <sub>0.5</sub>	IoU <sub>optimal</sub>	IoU <sub>M</sub>	GIoU <sub>0</sub>	GIoU <sub>optimal</sub>	GIoU <sub>M</sub>
F1	36.9 (24.8)	29.3 (19.7)	29.4 (26.0)	30.1 (18.1)	29.8 (18.6)	32.9 (25.5)
Hausdorff		45.4 (28.6)			47.6 (23.2)	
Wasserstein		19.6 (16.0)			21.7 (16.1)	
OSPA		14.5 (16.8)			15.7 (16.7)	

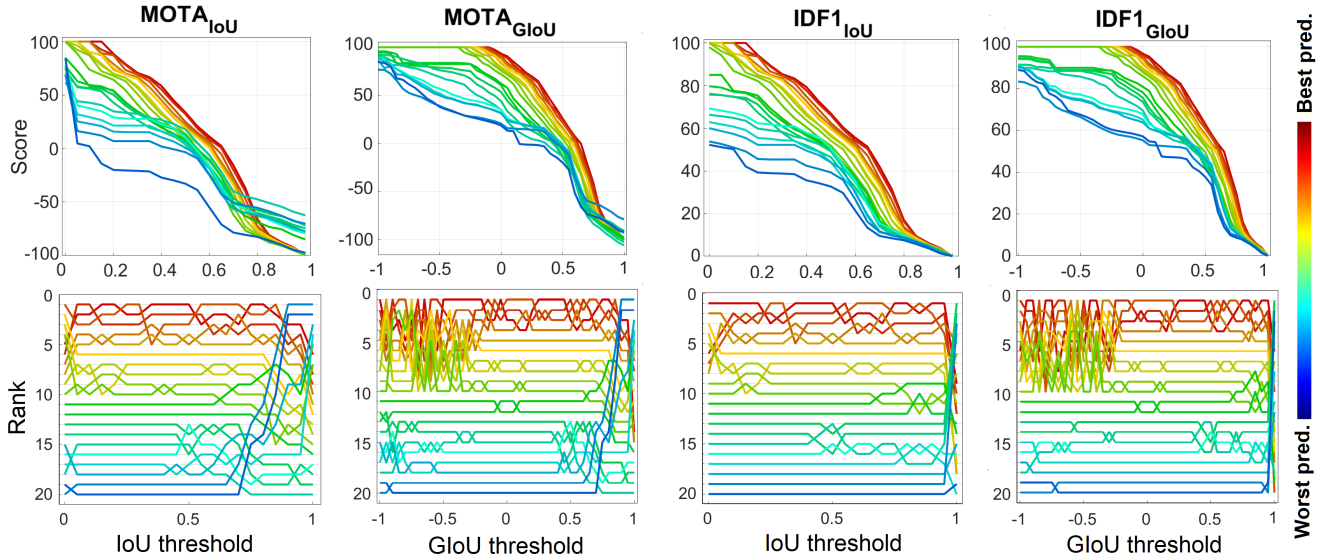


Figure 9: MOTA and IDF1 scores (top row) and the corresponding ranks of predictions (bottom row) over a range of IoU/GIoU thresholds in one trial of the multi-object tracking sanity test. The pre-determined ranks are color-coded from worst (blue) to best (red).

is governed by a function of the form  $\tau^{(k)}(n) = \alpha^{(k)} \times n$ . The constant  $\alpha^{(k)}$  is calculated by first forming a 20-D  $T$  vector whose elements are evenly spaced numbers between

10 and 20 (in the ascending order). The constant  $\alpha^{(k)}$  is then given as  $\alpha^{(k)} = T[k]/N_T$ .

For a track with label  $n$ , predicted by tracker  $k^{th}$  (at any

Table 4: Means (and standard deviations) of the ranking consistency indicators for traditional performance measures in multi-object tracking sanity test over all Monte Carlo trials.

Multi-object tracking test				
	MOTA <sub>IoU</sub>	IDF1 <sub>IoU</sub>	MOTA <sub>GIoU</sub>	IDF1 <sub>GIoU</sub>
$\overline{R_S}$	6.3 (1.0)	<b>4.3 (1.1)</b>	8.5 (1.1)	6.5 (1.1)
$\overline{R_{std}}$	3.5 (0.8)	2.2 (0.5)	3.1 (0.6)	<b>2.1 (0.4)</b>
$\overline{R_{std}}$	2.2 (0.3)	<b>2.0 (0.3)</b>	2.2 (0.2)	2.1 (0.2)

time step), the dislocation in x-coordinate of the centroid (over the entire length of the track) is  $\Delta_x^{(n,k)} = u \times \tau^{(k)}(n)$  where  $u$  is a random number sampled between 0 and 1. The dislocation in y coordinate of the centroid is then calculated as

$$\Delta_y^{(n,k)} = \sqrt{(\tau^{(k)}(n))^2 - (\Delta_x^{(n,k)})^2}. \quad (11)$$

For  $u_2$  be a 2-D vector whose elements are random number drawing between 0 and 1, if  $u_2[1] < 0.5$  then  $\Delta_x^{(n,k)} = -\Delta_x^{(n,k)}$  and if  $u_2[2] < 0.5$  then  $\Delta_y^{(n,k)} = -\Delta_y^{(n,k)}$ . We also add small uniform noise to the sizes of objects.

Similar to the detection sanity test, for the first 10 predictions sets we only introduce the disturbance on centroid location. From the 11<sup>th</sup> set, we start to introduce the mismatch in cardinality. We first sample the elements of the following 10-D vectors  $P_{fr}$  within the range  $[0.05, 0.95]$ ,  $P_{sft}$  within the range  $[0.05, 0.5]$ ,  $P_{rft}$  as Poisson random numbers with the rates of  $[1 : 1 : 10]$  and  $P_{id}$  within the range  $[0.05, 1]$ . We then sort elements of  $P_{fr}$ ,

$P_{sft}$  and  $P_{rft}$  in ascending order and  $P_{id}$  in descending order. The number of tracks with state-dependent falses is  $N_{sft} = N_T \times N_{sft}[k]$ . The tracks that have state-dependent falses (which are selected randomly) have an extra track with the same amount of dislocation from the true at each time step along their existing period as the predicted track. For a tracker  $k$ , at time  $t$ , the number of missed objects is  $N_{fr}^{(t,k)} = N^{(t,k)} \times P_{fr}[k]$ . The missed instances (tracks constituents) are chosen such that they have the highest values of the enumerated labels (worst prediction in terms of dislocation). To simulate the effect of identities swapping of the detected tracks, at each time step, we control the likelihood of swapping identities between tracks as following. First, we calculate the mutual IoU for all pairs of the tracks at current instance. The likelihood of the swapping event is governed by a S-shape membership function which takes mutual IoU as its argument and  $P_{id}[k]$  as its parameter. Specifically, for  $I^{(i,j)}$  is the mutual IoU between tracks instances labeled  $i$  and  $j$ , their identities swapping likelihood is given by Eqs. 12.

$$s(I^{(i,j)}, P_{id}[k]) = \begin{cases} 0 & I^{(i,j)} \leq 15 \\ 2 \times \left( \frac{I^{(i,j)} - 15}{P_{id}[k] - 15} \right)^2 & 15 \leq I^{(i,j)} \leq \frac{15 + P_{id}[k]}{2} \\ 1 - 2 \times \left( \frac{I^{(i,j)} - 15}{P_{id}[k] - 15} \right)^2 & \frac{15 + P_{id}[k]}{2} \leq I^{(i,j)} \leq P_{id}[k] \\ 1 & I^{(i,j)} \geq P_{id}[k] \end{cases}. \quad (12)$$

The tracks labels (at current time  $t$ ) are swapped if this likelihood is above 0.5 and the swapping procedure is carried out in the order from the pair with the highest to the lowest mutual IoU. Finally, for each tracker, we introduce  $P_{rft}[k]$  false tracks with fixed length of 5 time steps. The initial time are random, the initialization of false tracks is carried out the same way as of the reference tracks. During their active time, the centroids of false tracks also follow the constant velocity model while their sizes vary randomly within the range  $[20, 40]$  without any dynamic.

#### Extended results on the test

The MOTA and IDF1 scores (scaled up by 100 times) together with the corresponding ranks of predictions sets in

1 trial of the test are given in Fig. 9. The plots confirm the unreliability of the traditional criteria as the ranks switches severely over the range of thresholds, especially, at the higher end of the thresholds where the differences between the scores are narrow. The ranking consistency indicators are given in Tab. 4 which demonstrates that IDF1 criterion is generally more reliable than the MOTA criterion for all ranking consistency indicators over all trials of the test. In particular, IDF1 score with IoU base measure is more reliable than its GIoU counterpart given it has lower average number of ranking switches and lower sensitivity to the change in hyper-parameter.

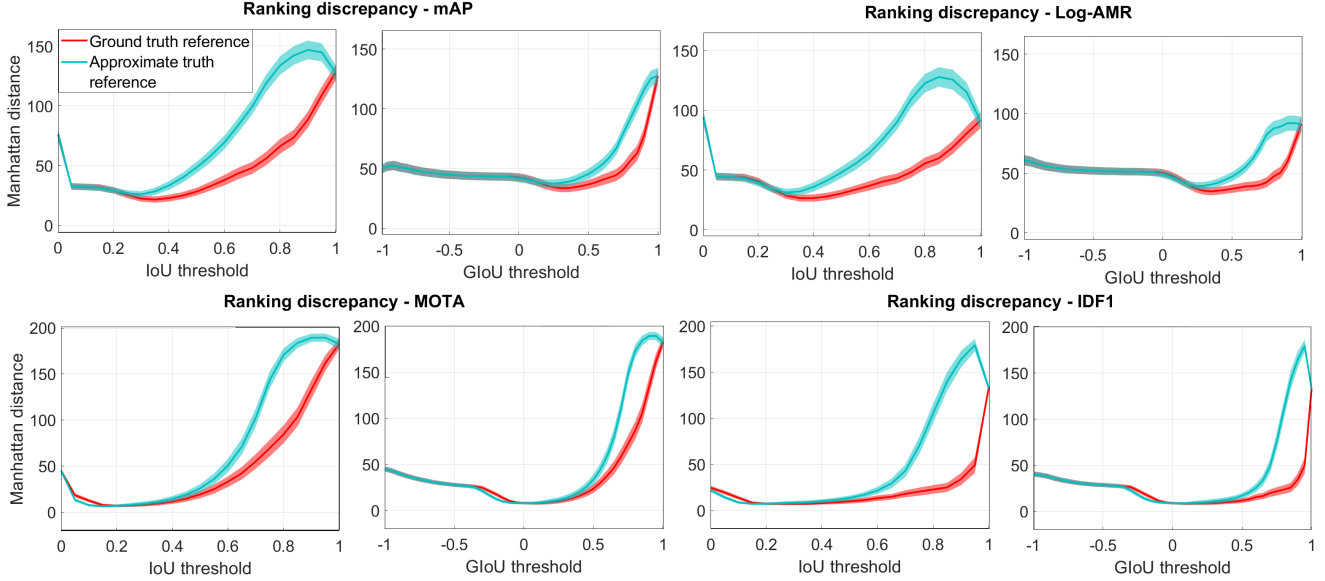


Figure 10: Mean Manhattan ranking errors (from the true ranking) of various traditional criteria at different thresholds with ground truth and approximate truth reference sets, over all Monte Carlo trials in **detection test (top row)** and **tracking test (bottom row)**. Shaded area around each curve indicates 0.2-sigma bound.

Table 5: Means (and standard deviations) of Manhattan ranking errors of various metric criteria with ground truth and approximate truth reference sets, over all Monte Carlo trials.

Multi-class multi-object detection test						
	Hausdorff		Wasserstein		OSPA	
	IoU	GIoU	IoU	GIoU	IoU	GIoU
Ground truth reference	23.5 (18.8)	25.0 (13.6)	14.1 (18.5)	15.7 (13.6)	9.81 (13.0)	12.1 (13.7)
Approximate truth reference	28.4 (17.7)	28.8 (13.0)	19.9 (17.7)	19.9 (13.0)	15.7 (13.0)	16.3 (13.2)
Multi-object tracking test						
	Hausdorff( $\tilde{d}$ )		Wasserstein( $\tilde{d}$ )		OSPA( $\tilde{d}$ )	
	IoU	GIoU	IoU	GIoU	IoU	GIoU
Ground truth reference	14.2 (9.1)	17.2 (9.2)	3.7 (3.7)	4.9 (4.0)	2.5 (2.3)	2.8 (2.5)
Approximate truth reference	15.9 (9.2)	18.3 (9.4)	5.5 (4.3)	6.4 (4.5)	4.2 (3.0)	4.2 (3.1)

### D.3. Further illustration on the importance of mathematical consistency

To illustrate the effect of mathematical inconsistency on different performance measures, we set up the following experiment. First, we generate the ground truth and prediction sets for the multi-class multi-object detection and multi-object tracking tests as in previous experiments. In addition, we also generate sets of approximate truth which are the same as the ground truth sets except the bounding boxes are dislocated by a random small amount (the minimum allowable IoU index between ground truth and approximate truth is 70%). We then compute the Manhattan distance between the true ranking vector and ranking vectors evaluated

via using ground truth and approximate truth references. The results for traditional criteria are shown in Fig. 10 and the ones for metrics criteria are shown in Tab. 5.

The results indicate that for the traditional criteria, the Manhattan distance between the prediction and the approximate truth is substantially higher than of the Manhattan distance between the prediction and the ground truth at high thresholds of IoU and GIoU. It can be explained as because there is less similarity between the predicted boxes and the approximate true boxes, the correct predictions are ignored completely (although they might have good overlap with the true boxes). For the metrics criteria, we observe the difference in Manhattan distance for ground truth and approximate

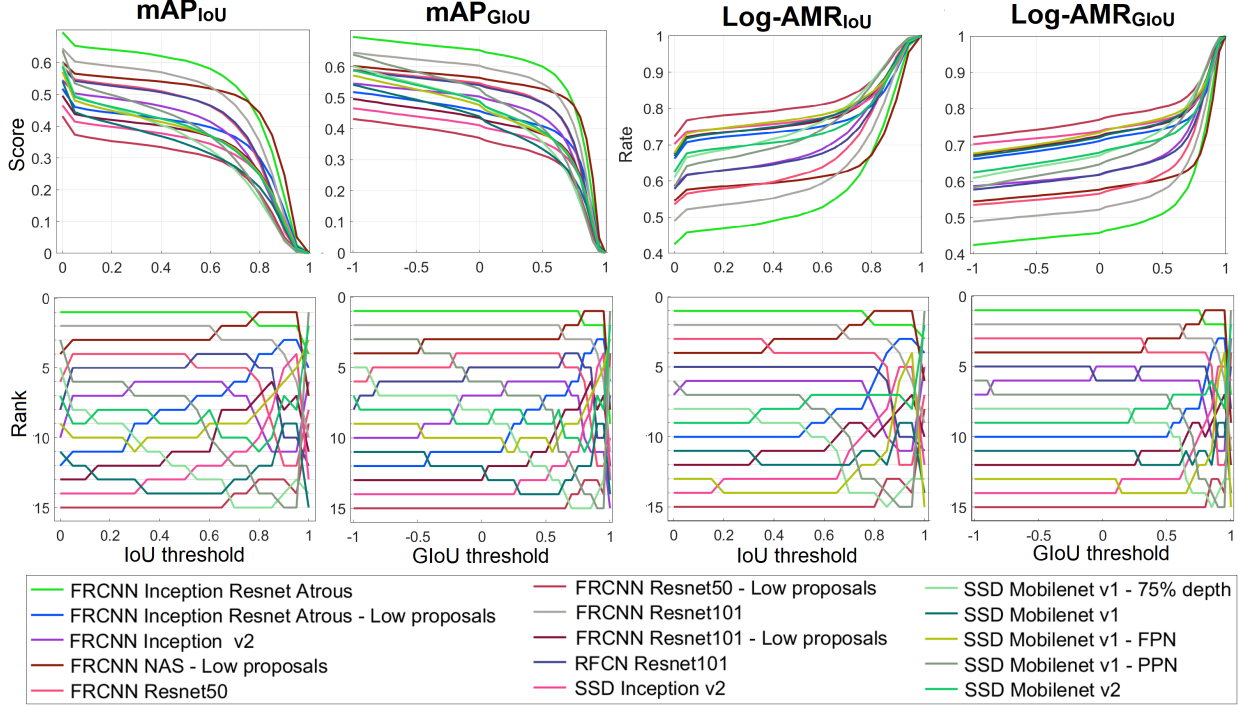


Figure 11: Score/rate and ranks of predictions sets according to mAP and log-AMR over range of IoU/GIoU thresholds in COCO bounding box detection experiment.

Table 6: Ranking consistency indicators for traditional performance measures in COCO bounding box detection experiment.

COCO bounding box detection				
	mAP <sub>IoU</sub>	Log-AMR <sub>IoU</sub>	mAP <sub>GIoU</sub>	Log-AMR <sub>GIoU</sub>
$\overline{R_S}$	5.3	<b>4.5</b>	6.0	4.7
$\overline{R_{std}}$	2.1	2.0	2.0	<b>1.6</b>
$\overline{R_{Sen}}$	<b>5.26</b>	5.41	5.7	5.6

truth references is insignificant. It is expected due to the small distance between the ground truth and approximate truth. It is hence demonstrated that without mathematical consistency, if only the approximate truth is available as reference, the meaningfulness is not guaranteed for traditional criteria, *i.e.*, ranking via evaluating predictions against the approximate truth might be very different from the ranking evaluating against the ground truth at certain thresholds while the difference is less severe if the metrics properties hold.

#### D.4. Results on real dataset

In this section, we show the detailed results on each real dataset experiment, *i.e.*, COCO detection with bounding box, COCO instance level segmentation and MOTChallenge multi-object tracking to supplement Section 5.2 of the main text.

##### D.4.1 COCO bounding box detection

In addition to the ranking plot in the main text, in this subsection, we provide the plots of the scores and the details on how the ranks vary across different IoU/GIoU thresholds in Fig. 11. Over thresholds ranges, we observe that the ranks gradually change. For example, the “SSD Mobilenet v1 - 75% depth” performs relative well at low threshold but gradually gets worse when the threshold increases or the “FRCNN Inception Resnet Atrous - Low Proposals” performs worse at low thresholds but gets better at higher thresholds. In general, at low thresholds, we observe the ranks are quite stable but from value of 0.6 onward (both IoU and GIoU) the ranks start to switch more frequently. This observation is also confirmed in the log-AMR plot in Fig. 7 of [17]. In Tab. 6, we show the ranking consistency indicators of different criteria. In general, log-AMR performs relatively more reliable comparing to the mAP although it is slightly more sensitive to the change in thresholds comparing to mAP with IoU base measure.

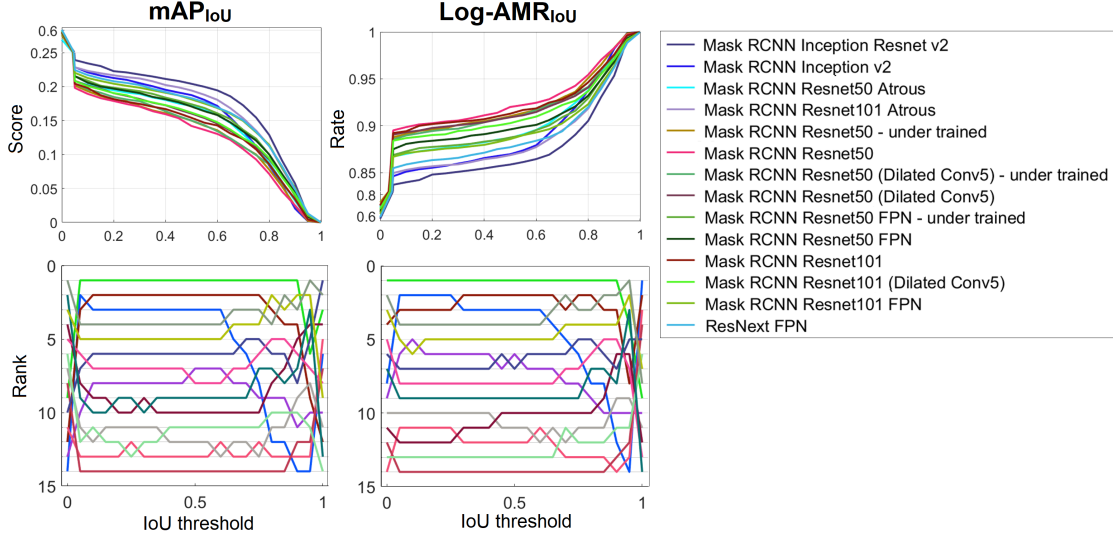


Figure 12: Score/rate and ranks of predictions sets according to mAP and log-AMR criteria over range of IoU thresholds in COCO instance level segmentation experiment.

Table 7: Ranking consistency indicators for traditional performance measures in COCO instance level segmentation experiment.

COCO instance level segmentation		
	mAP <sub>IoU</sub>	Log-AMR <sub>IoU</sub>
$\overline{R_S}$	4.5	4.0
$\overline{R_{std}}$	1.9	1.7
$\overline{R_{Sen}}$	3.6	3.6

#### D.4.2 COCO instance level segmentation

Similar to the previous experiment, we provide further details on the scores and ranks in the COCO instance level segmentation experiment in Fig. 12. It is observed that the ranking order is unstable over the range of thresholds, especially, at high value thresholds. The ranking consistency indicators given in Tab. 7 shows log-AMR is more reliable than the mAP score.

#### D.4.3 MOTChallenge tracking

In this experiment, the ranks switch frequently across different thresholds as shown in Fig. 13. Especially, it is noticeable that the “jCC” method changes the rank dramatically after threshold of 0.5 (from the 4<sup>th</sup> to the last at IoU threshold of 0.7). We observe higher number of switches at the high extreme of the thresholds ranges which indicates the criteria are more unreliable at high thresholds. From Tab. 8, it can be shown that IDF1 is relatively more reliable comparing to MOTA but it is slightly more sensitive to the change of IoU thresholds.

#### D.5. Optimal assignment approach for mAP and log-AMR

In this experiment, we construct the sanity test in the like-wise manner to the mentioned multi-class multi-object detection experiment. We then evaluate the predictions sets on the standard mAP, log-AMR criteria (with greedy assignment) and their corresponding optimal assignment approach. In Fig. 14 and Fig. 15, by visual inspection, it is observed that the ranks switch severely for both greedy and optimal assignments approaches in a particular trial. However, in Tab. 9 it is confirmed that the optimal assignment approach is more reliable than greedy counterpart although it is not the case for log-AMR with GIoU base measure.

In terms of the meaningfulness of the ranks, the optimal assignment approach is better than the greedy one in terms of ranking accuracy as shown in Fig. 16. For the proposed approach, while it is competitive to the Hausdorff metric, it is still less meaningful than the Wasserstein and OSPA metrics. Tab. 10 further confirms that optimal is better than greedy assignment approach as it produces more meaningful ranking order. For both greedy and optimal assignment approaches, the marginalization of thresholds does not always produce more meaningful ranking order comparing to the optimal threshold which is due to the strong dependency of the scores/rates on the thresholds.



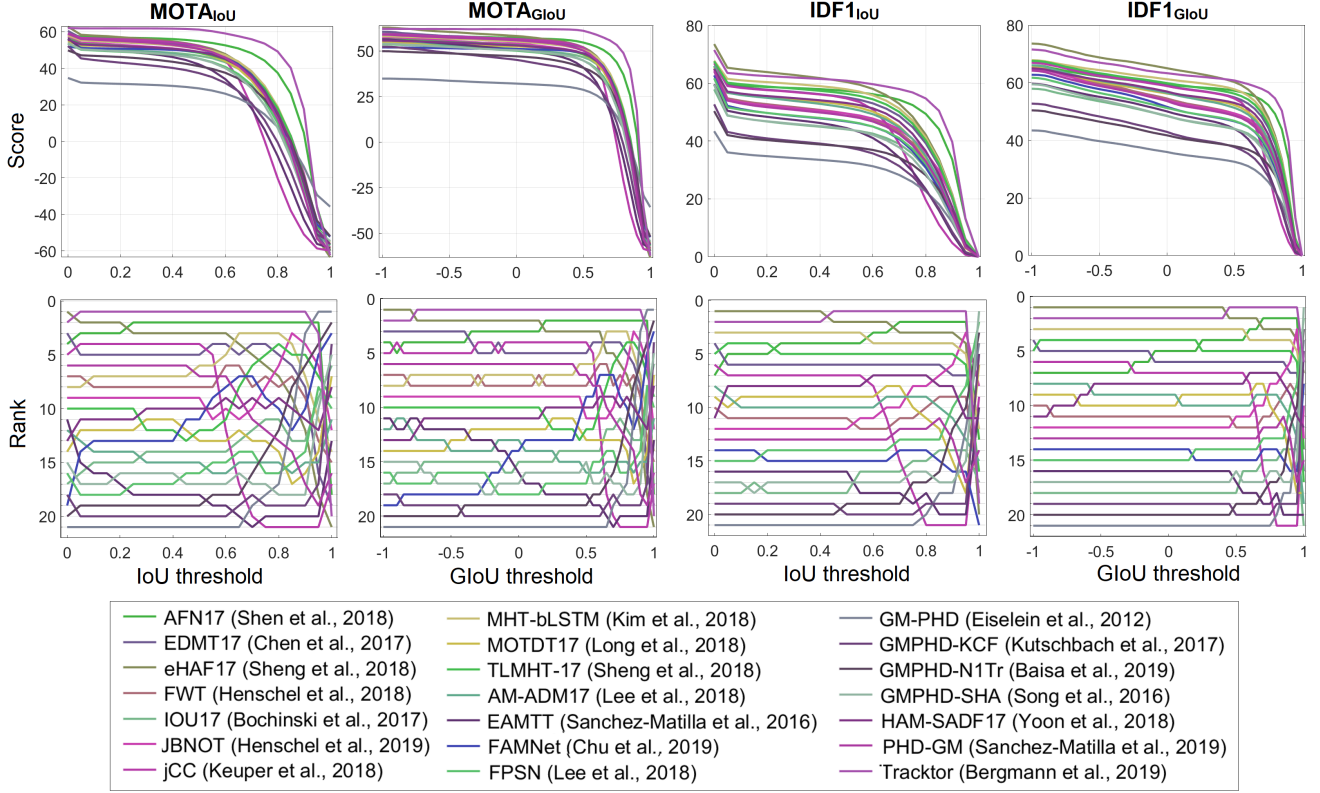


Figure 13: Score/rate and ranks of predictions sets according to MOTA and IDF1 over range of IoU/GIoU thresholds in MOT17 tracking experiment.

Table 8: Ranking consistency indicators for MOTA and IDF1 in MOT17 tracking experiment.

MOT17 multi-object tracking				
	MOTA <sub>IoU</sub>	IDF1 <sub>IoU</sub>	MOTA <sub>GIoU</sub>	IDF1 <sub>GIoU</sub>
$\overline{R_S}$	6.5	<b>4.2</b>	7.9	5.8
$\overline{R_{std}}$	3.5	2.7	3.5	<b>2.2</b>
$\overline{R_{Sen}}$	<b>5.1</b>	5.4	5.6	5.6

Table 9: Means (and standard deviations) of the ranking consistency indicators for mAP and log-AMR with greedy and optimal assignment approaches over all Monte Carlo trials.

mAP and log-AMR with optimal assignment				
	mAP <sub>IoU</sub>	mAP <sub>IoU</sub> -optimal	mAP <sub>GIoU</sub>	mAP <sub>GIoU</sub> -optimal
$\overline{R_S}$	8.1 (1.1)	<b>7.3 (1.4)</b>	8.6 (1.3)	8.9 (1.5)
$\overline{R_{std}}$	3.5 (0.6)	3.1 (0.8)	<b>2.7 (0.5)</b>	2.7 (0.6)
$\overline{R_{Sen}}$	3.6 (0.7)	3.2 (0.8)	3.4 (0.6)	<b>3.0 (0.6)</b>
	Log-AMR <sub>IoU</sub>	Log-AMR <sub>IoU</sub> -optimal	Log-AMR <sub>GIoU</sub>	Log-AMR <sub>GIoU</sub> -optimal
$\overline{R_S}$	7.9 (1.0)	<b>6.9 (1.2)</b>	8.7 (1.3)	8.9 (1.5)
$\overline{R_{std}}$	3.2 (0.6)	2.7 (0.6)	<b>2.6 (0.5)</b>	2.6 (0.6)
$\overline{R_{Sen}}$	3.5 (0.6)	<b>3.1 (0.6)</b>	3.5 (0.6)	<b>3.1 (0.6)</b>

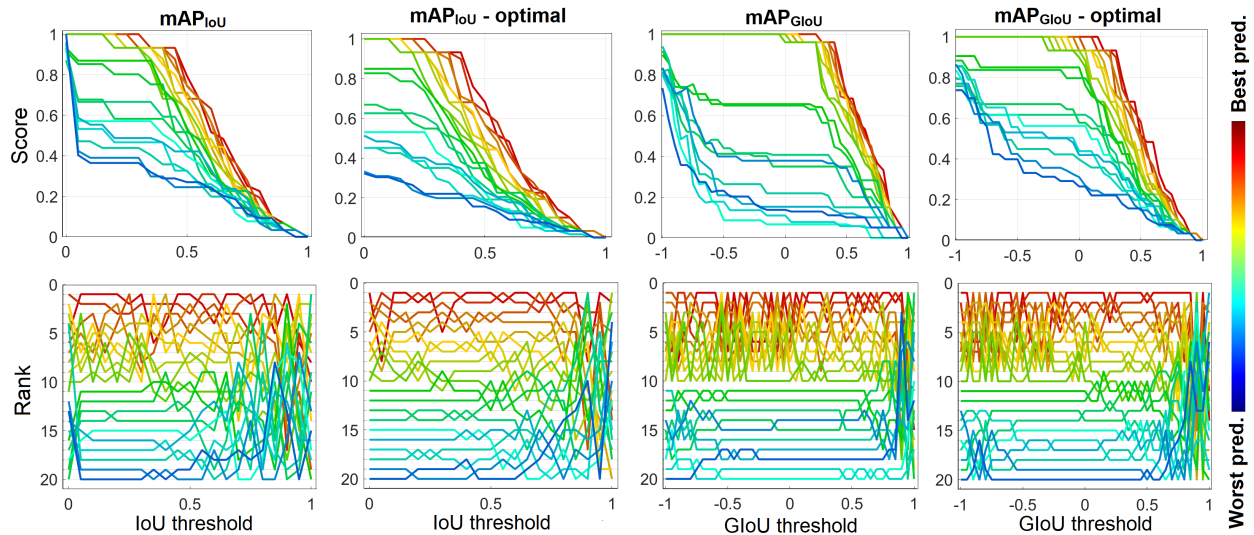


Figure 14: mAP scores with greedy and optimal assignment approaches (top row) and the corresponding ranks of predictions (bottom row) over a range of IoU/GIoU thresholds in one trial of the multi-class multi-object detection sanity test. The pre-determined ranks are color-coded from worst (blue) to best (red).

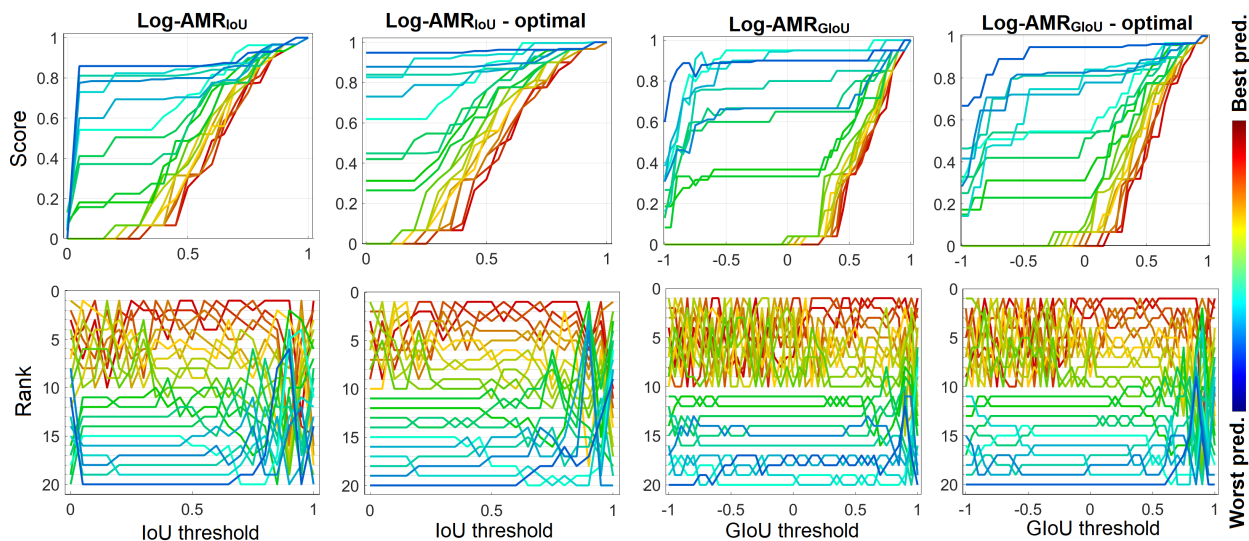


Figure 15: Log-AMR with greedy and optimal assignment approaches (top row) and the corresponding ranks of predictions (bottom row) over a range of IoU/GIoU thresholds in one trial of the multi-class multi-object detection sanity test. The pre-determined ranks are color-coded from worst (blue) to best (red).

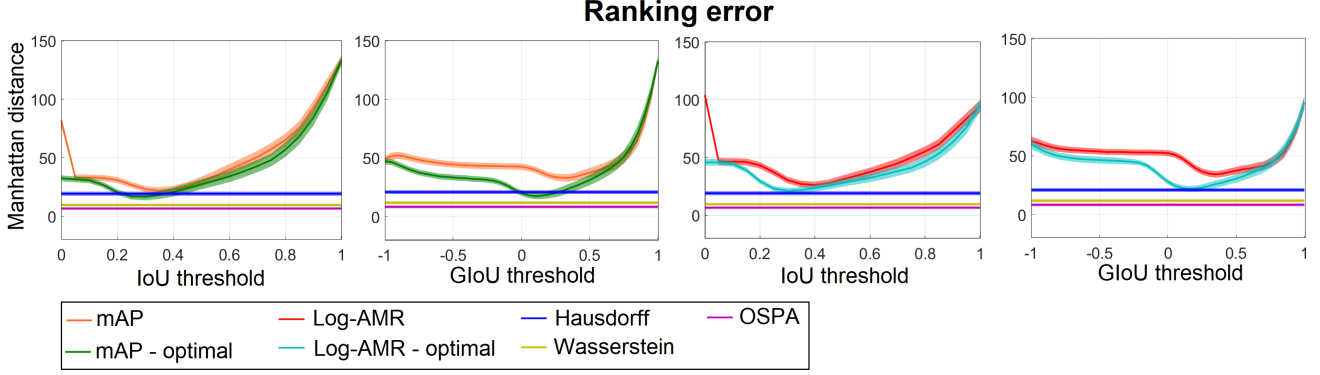


Figure 16: Mean Manhattan ranking errors (from the true ranking) of various criteria at different thresholds, over all Monte Carlo trials in multi-class multi-object detection test with greedy and optimal assignment approaches. Shaded area around each curve indicates 0.2-sigma bound. We also show the results for metrics criteria for reference.

Table 10: Means (and standard deviations) of Manhattan ranking errors of mAP and log-AMR with greedy and optimal assignment approaches at certain thresholds, over all Monte Carlo trials. The subscripts of IoU/GIoU indicate the threshold values; "optimal" threshold is the one with best ranking accuracy; "M" threshold indicates that the evaluation is done via averaging the score over the range 0.5 to 0.95 in steps of 0.05. We also show the results for metrics criteria for reference.

mAP and log-AMR with optimal assignment						
	IoU <sub>0.5</sub>	IoU <sub>optimal</sub>	IoU <sub>M</sub>	GIoU <sub>0</sub>	GIoU <sub>optimal</sub>	GIoU <sub>M</sub>
mAP	29.6 (20.4)	21.9 (14.3)	<b>18.9 (19.8)</b>	42.5 (13.4)	33.1 (16.3)	30.6 (19.9)
mAP-optimal	<b>27.3 (21.5)</b>	<b>16.7 (14.7)</b>	19.0 (20.2)	<b>20.0 (11.4)</b>	<b>17.9 (14.5)</b>	<b>20.8 (21.3)</b>
Log-AMR	31.1 (17.4)	26.3 (14.4)	23.9 (15.5)	52.4 (13.0)	34.9 (13.6)	28.2 (11.9)
Log-AMR-optimal	<b>27.9 (16.1)</b>	<b>21.1 (12.0)</b>	<b>21.3 (14.6)</b>	<b>28.0 (10.8)</b>	<b>24.3 (14.6)</b>	<b>20.1 (8.47)</b>
Hausdorff		19.3 (9.0)			20.9 (8.0)	
Wasserstein		9.6 (5.9)			11.8 (6.9)	
OSPA		6.6 (5.5)			8.3 (6.2)	

## References

- [1] M. Beard, B.-T. Vo, and B.-N. Vo. A solution for large-scale multi-object tracking. *IEEE Transactions on Signal Processing*, 68:2754–2769, 2020.
- [2] K. Bernardin and R. Stiefelhagen. Evaluating multiple object tracking performance: The clear mot metrics. *Journal on Image and Video Processing*, 2008:1, 2008.
- [3] R. L. Dobrushin. Prescribing a system of random variables by conditional distributions. *Theory of Probability & Its Applications*, 15(3):458–486, 1970.
- [4] P. Dollar, C. Wojek, B. Schiele, and P. Perona. Pedestrian detection: An evaluation of the state of the art. *IEEE Transactions on Pattern Analysis and Machine Intelligence*, 34(4):743–761, 2011.
- [5] M. Everingham, L. Van Gool, C. Williams, J. Winn, and A. Zisserman. The pascal visual object classes (voc) challenge. *International Journal of Computer Vision*, 88(2):303–338, 2010.
- [6] B. Grunbaum. *Convex polytopes*. Interscience, 1967.
- [7] J. R. Hoffman and R. P. S. Mahler. Multitarget miss distance via optimal assignment. *IEEE Transactions on Systems, Man, and Cybernetics - Part A: Systems and Humans*, 34(3):327–336, 2004.
- [8] T.-Y. Lin, M. Maire, S. Belongie, J. Hays, P. Perona, D. Ramanan, P. Dollar, and C. L. Zitnick. Microsoft coco: Common objects in context. In *European Conference on Computer Vision (ECCV)*, 2014.
- [9] H. Rezatofighi, N. Tsoi, J. Gwak, A. Sadeghian, I. Reid, and S. Savarese. Generalized intersection over union: A metric and a loss for bounding box regression. In *Conference on Computer Vision and Pattern Recognition (CVPR)*, 2019.
- [10] E. Ristani, F. Solera, R. Zou, R. Cucchiara, and C. Tomasi. Performance measures and a data set for multi-target, multi-camera tracking. In *European Conference on Computer Vision (ECCV)*, 2016.
- [11] D. Schuhmacher, B.-T. Vo, and B.-N. Vo. A consistent metric for performance evaluation of multi-object filters. *IEEE Transactions on Signal Processing*, 56(8):3447–3457, 2008.